Electron-gas theory of ionic crystals, including many-body effects

Carl Muhlhausen and Roy G. Gordon
Department of Chemistry, Harvard University, Cambridge, Massachusetts 02138
(Received 17 January 1980)

The electron-gas theory of ionic crystals is extended to include nonadditive (many-body) interactions arising from the simultaneous overlap of the densities of several ions. The theory is used to predict equilibrium geometries, lattice energies, and pressure-induced phase transitions for the fluorides and oxides of the alkali and alkaline earth metals. The results are in good agreement with electron-gas calculations assuming additive, two-body interactions between pairs of ions. This comparison shows that the simultaneous overlap of three or more ions has only a small effect on these crystals, and that for many purposes the simpler two-body approximation is adequate. The predictions of lattice distances and energies agree with experiment to a typical accuracy of 1 or 2%. In order to obtain this accuracy, it is necessary to calculate the electron densities for the anions in a stabilizing potential well whose size is determined self-consistently by the electrostatic potential of the crystal at the anion site. This shrinkage of the anion by the crystal is also a kind of many-body interaction, but it can be handled within the framework of an effective two-body interaction involving the stabilized anions. The corresponding cation expansion effect is also calculated, and shown to be negligible for the alkali and alkaline earth metal ions.

I. INTRODUCTION

The development of an adequate theory for the structure and binding in crystals has been a problem in solid-state science for many years. Such a theory should not only give good agreement with existing experimental data, it should also be of predictive value and be applicable to systems and situations which are experimentally inaccessible.

To date, the most widely applied theories have been of the semi-empirical Born-Mayer type,[1,2] in which the binding in solids is described as sums of pair interactions. The forces between pairs are written in terms of an interaction potential with variable parameters which are usually determined by empirical fitting to experimental data. With a careful selection of a flexible pair potential, the Born-Mayer model can give good agreement with a large variety of experimental results, but because it is an essentially empirical model, pair potential parameters determined with one set of experimental data may give poor results when used to calculate the properties of other systems. The range of applicability of the Born-Mayer model is severely limited by the experimental data available.

A purely *ab initio* theoretical model would not suffer from these defects. In practice, however, most quantum-mechanical models[3,4] have been too complex to be applied to any but the simplest solid-state systems. Often the mathematical difficulties encountered and approximations introduced to surmount these difficulties make rigorous quantum-mechanical theories of limited practical value.

Perhaps the most promising *a priori* theory of recent years is the electron-gas theory of Gordon and Kim (GK).[5(a)] Although originally used for molecular systems, it has been successfully applied to a number of simple ionic crystals.[5(b)] This theory has been the subject of much interest and a modified version[6] has been found to give excellent agreement with the known structures and binding energies of the alkali halides[7(a)] and alkaline earth oxides.[7(b)] In addition, the theory was used to calculate the compressibilities, elastic constants, and high-pressure behavior of these systems. In contrast to other quantum-mechanical theories, the electron-gas theory is easily applied to larger and more complex systems. It holds much promise for further development and extension to a wide variety of solid-state problems.

In their treatments of ionic crystals, Kim and Gordon[5(b)] and Cohen and Gordon (CG)[7] expressed the binding energy of the crystal as the sum of a point Coulomb or Madelung energy term and a short-range contribution which was written as a sum of pair interactions. The short-range interactions were determined by the electron-gas theory. The major features of the original GK[5] theory and the later modified electron gas (MEG) theory[6] are that the short-range pair interaction energy is split into kinetic, exchange, correlation, and nonpoint Coulomb electrostatic contributions, and each of these is written as a relatively simple functional of the electron densities. The net electron density of an interacting pair is taken as a superposition of the atomic densities, which are calculated from Hartree-Fock atomic wave functions.

The model is similar to the Born model in that the binding energy of the crystal is written as a sum of pair interactions, and many-body effects are neglected. However, no empirical parameters are introduced. The systems treated were of high symmetry, where the energy could be written as a function of a single lattice constant, and the structure determined by minimizing the energy with respect to this parameter.

This approach can be readily extended to any crystal where the binding energy can be written as a sum of pair interactions between the atomic components. Since the short-range energy will depend only upon the distances between pairs, the binding energy will in general depend upon the six lattice constants and the positions of each ion in the unit cell. The structure can be determined by minimizing the energy with respect to these geometrical parameters.

Such a model would still ignore many-body contributions to the energy, which are the deviations of the net interaction energy of a many-atom system from the pairwise additive approximation. In the electron-gas theory there are three types of many-body contributions. The first type manifests itself in the nonlinearity of the density functionals for the kinetic, exchange, and correlation energies.[8] The second and third types of many-body effects are due to two types of changes an atomic charge density undergoes in the presence of the other charges in the system. Changes in the electron charge densities from their gas phase forms will affect all of the electron-gas interaction energies including the Coulomb energy, which once the densities are fixed, is pairwise additive. These changes in the charge densities are of two types:

(1) Size changes which retain the net spherical symmetry of the charge densities.

(2) Polarizations or distortion of the electron densities from spherical symmetry leading to dipolar or higher-order multipole interactions in the system.

The size changes were incorporated into the theory[7(b),9] by determining electron-gas pair potentials from spherical Hartree-Fock charge densities which were stabilized by including a Madelung potential term in the Hamiltonian. This is a means of accounting for size change many-body effects. Dipolar distortions were also included[9] by means of a shell model.[9,10] The model was applied[7,9] to a number of ionic halide and oxide crystals and excellent results were obtained for most of the systems treated. Unfortunately, it is not clear whether the energy differences between the gas phase and the stabilized anions were included in the latest calculations[9] of the cohesive energies in these systems. In addition, they[9] report "cohesive energies" for oxide crystals which are the energies necessary to separate the crystals into gaseous cations and O^{2-} anions. These results are compared to "experimental" cohesive energies. As was discussed in detail by CG,[7(b)] there are several inconsistencies in this type of comparison. Since gaseous O^{2-} is unstable, electron-gas lattice energy calculations for oxides must employ stabilized wave functions of some variety. The calculated cohesive energies then refer to the energy required to separate the crystal into the stabilized anions, not gas phase ions. The "experimental" cohesive energies, determined from thermochemical data, are also incomplete. Experimentally, oxide crystals can dissociate into free O^- ions not O^{2-} ions. Values for the energy change in the process $O^{2-}(g) \rightarrow O^-(g) + e^-$, which are needed to complete the thermodynamic cycle, have been reported,[11,12] but these are based in part on Born-Mayer lattice energy calculations, which are themselves suspect.

A more appropriate quantity, which is experimentally accessible, is the energy necessary to separate an oxide crystal into free O^- ions, free electrons, and free positive ions. We will return to this point later in Sec. V.

The pairwise additive approximation could be extended to crystals where the binding is between molecular units if the pair potentials were expressed as functions of the distance between units and their mutual orientation. Such a model becomes cumbersome, however, and difficult to use since completely general methods for calculating the interaction energy between a pair of molecules by the electron-gas theory have not yet been developed. Once again, nonadditive many-body effects, thought to be important in describing the binding in many crystals,[13] would be neglected.

In this paper we present a general electron-gas theory for the binding in crystals, based on the MEG theory, which includes nonadditive and size change many-body effects. No empirical parameters are introduced into the theory and it is applicable to any atomic ionic crystal. The method is readily extended to molecular crystals.[14] For the present we confine ourselves to systems of relatively high symmetry and ignore polarization effects.

The relevant equations used to calculate the crystal binding energy by the MEG theory are derived in Sec. II and a general technique for calculating the electrostatic interaction in crystals is presented. Details of the numerical methods used to calculate the binding energy are given in Sec. III, along with techniques for handling multidimensional numerical integrations. In Sec. IV, we discuss a method, similar to that used in Refs. 7(b) and 9, for incorporating size changes of the anion densities in the crystal energy calculations. In Sec. V, a self-consistent scheme for including this effect in the calculations is proposed. In addition, we discuss theoretically calculated energy cycles which are appropriate for halide and oxide crystals and may be directly compared to experimental quantities.

In this paper, we test the model on a representative selection of highly ionic fluorides and oxides and compare calculated equilibrium geometries and dissociation energies with experiment. The importance of size change and nonadditive many-body effects is assessed by comparison of our results with previous results[7(a),7(b)] obtained from gas phase fluoride and partially stabilized oxide wave functions in a pairwise additive approximation. The predictive value of the theory is also tested by calculations of relative stability of alternative structures for these systems. Results of the theory for more complex and less ionic crystals will be published at a later time.

The theory is first applied to LiF, NaF, MgO, and CaO in Sec. VI A. The results are in excellent agreement with experimental energies and geometries and are significantly improved over the CG[7] results for these systems. The results of calculations for these systems in the $B2$ (cesium chloride) and $B3$ (sphalerite) structures are given in Sec. VI B. The method gives the correct relative stability for these structures for all but LiF, which is found to be most stable in the $B3$ form. Possible sources of this error are considered.

The results of calculations on BeF_2, MgF_2, CaF_2, and Na_2O are given in Sec. VII. The calculated results for dissociation energies and geometries of the observed structures are in close agreement with the experimental values. Comparison of the observed structures with a number of simple alternative structures is made. For all these systems, except CaF_2, the model predicts the correct structure. In CaF_2, a rutile structure is calculated to be slightly more stable than the observed fluorite structure. The pressure-induced phase transition is calculated for MgF_2, from the normal rutile form to the high-pressure fluorite form. The transition pressure and the pressure-volume equation of state are in reasonable agreement with experiment.

II. ELECTRON-GAS MODEL FOR CRYSTALS

In this section expressions for the crystal binding energy, including nonlinear many-body interactions, are derived from the MEG density functionals. We work within the static lattice approximation and consider a set of *fixed* charge densities in a given crystalline arrangement. We then define the binding energy, W_B, as the crystal interaction energy relative to the self-energies of the infinitely separated, fixed charge densities. These charge densities may not be experimentally observable species and thus W_B is not, in general, an experimentally measurable quantity. The connection between W_B and experimental dissociation energies will be made in Sec. V.

In the electron-gas theory we separate the binding energy, W_B, into four contributions such that

$$W_B = (W_E + W_K + W_X + W_C)/n \quad , \tag{1}$$

where W_E is the electrostatic interaction energy per unit cell and n is the number of formula units in the unit cell. The remaining terms in Eq. (1) are, respectively, the kinetic, exchange, and correlation interaction energies per unit cell, which are calculated by the MEG theory.

As our first approximation, we assume that the total electron density in the crystal can be written as a superposition of the density of the individual units,

$$\rho_E(\vec{x}) = \sum_i \sum_{\vec{l}} \rho_i(\vec{x} - \vec{r}_{il}) \quad , \tag{2}$$

where the sum over i in this and all subsequent expressions extends over the individual charge distributions in the unit cell. The vector $\vec{r}_{il}$ points to the center of a charge distribution in the crystal and may be written as

$$\vec{r}_{il} = \vec{r}_i + \vec{r}_l \quad ,$$

where $\vec{r}_i$ locates a charge distribution in the unit cell nearest the origin and $\vec{r}_l$ is a lattice translation vector. The sum over $\vec{l}$ in Eq. (2) extends over all unit cells. For simplicity we will take the $\rho_i(x)$ to be spherically symmetric charge densities, although most of the following is easily adapted to the case of nonspherical molecular charge densities.

For the present we make no assumptions about the spherical charge densities; they may be determined from gas phase or stabilized wave functions of some sort. Then $-W_B$ refers to the energy necessary to bring these charge densities to infinite separation. In order to derive an expression for the binding energy as a functional of the charge density, it is most convenient to treat the three electron-gas energy terms separately from the electrostatic term.

A. Electron-gas interaction energies

In the various electron-gas theories the total kinetic, exchange, or correlation energy of a system of electrons may each be written as an integral of the energy-density functional for that term. The energy density is a functional of the total electron density. For a crystal, if the integral is written as extending over a unit cell, the total energy per unit cell, including the effects of nonadditive many-body forces, is obtained. The interaction energy for a given term results when the self-energies of the individual charge densities are subtracted from the total energy.

Let W denote one of the three interaction terms, W_K, W_X, or W_C, and $\mathcal{E}(\rho(x))$ be the energy density functional appropriate to that term. The electron-gas interaction energy per unit cell is then

$$W = \int_V d\vec{x}\, \mathcal{E}(\rho_E(x)) - \sum_i \int d\vec{x}\, \mathcal{E}(\rho_i(\vec{x} - \vec{r}_i)) \quad , \tag{3}$$

where $\rho_E(\vec{x})$, Eq. (2), is the total electron density from all the overlapping charge distributions. The subscript V on the first integration sign indicates an integration over a single unit cell of volume V. The remaining integrations are over all space and account for the self-energies of the individual electronic densities. For the kinetic, exchange, and correlation terms, respectively, the density functionals are[5(a)]

$$\mathcal{E}_K(\rho) = \tfrac{3}{10}(3\pi^2)^{2/3} C_K \rho^{5/3} \ , \tag{4a}$$

$$\mathcal{E}_X(\rho) = -\tfrac{3}{4}(3/\pi)^{1/3} C_X \rho^{4/3} \ , \tag{4b}$$

$$\mathcal{E}_C(\rho) = \begin{cases} C_C(-0.438 r_s^{-1} + 1.325 r_s^{-3/2} - 1.47 r_s^{-2} - 0.4 r_s^{-5/2})\rho, & r_s \geq 10.0 \\ C_C(0.018\,98 \ln r_s - 0.061\,56)\rho, & 0.7 \leq r_s \leq 10.0 \\ C_C(0.0311 \ln r_s - 0.048 + 0.009 r_s \ln r_s - 0.01 r_s)\rho, & r_s \leq 0.7 \end{cases} \ , \tag{4c}$$

where $r_s = (3/4\pi\rho)^{1/3}$. The coefficients C_K, C_X, and C_C are the correction factors introduced in the MEG theory.[6]

The integrations indicated in Eq. (3) must be performed numerically. Because each of the terms is large, there will be considerable loss of accuracy if they are separately integrated and then combined. It is far more efficient if all the terms are combined into a single integrand so that the interaction energy is obtained directly. This is achieved by converting the self-energy terms into integrations over a unit cell.

First we can write Eq. (3) as

$$W = \int_V dx \mathcal{E}(\rho_E(\vec{x})) - \sum_i \sum_{\vec{l}} \int_{V_l} dx' \ (\rho_i(\vec{x}' - \vec{r}_i)) \ ,$$

where in the second term the integrations over space have been converted into a lattice sum of integrations over unit cells. The subscript V_l indicates that we integrate over the unit cell with origin at r_l. A change of variables to $x = x' - r_l$ and a relabeling of the lattice indices yields

$$W = \int_V dx \left[\mathcal{E}(\rho_E(\vec{x})) - \sum_i \sum_{\vec{l}} \mathcal{E}(\rho_i(\vec{x} - \vec{r}_{il})) \right] \ . \tag{5}$$

Each of the electron-gas interaction energies can thus be calculated in a single three-dimensional quadrature over a unit cell of the crystal. Since the electron densities fall off rapidly with distance, the indicated lattice sums are easily performed. By choosing the cutoffs for the density summations so that the energy terms have converged, we include all the neighbors that contribute to the binding. Since the density functionals are nonlinear in the density, nonadditive many-body effects are incorporated into the model with no further effort.

B. Electrostatic interaction energy

Because of the long-range Coulomb forces in an ionic crystal the electrostatic interactions are more difficult to calculate than the short-range electron-gas terms. We have developed a method, which is similar to the double sum formula of Ewald[15] for the point Coulomb interactions, that evaluates the electrostatic energy as sums in the direct and reciprocal lattice, and a numerical integration that is conveniently combined with the integration of the electron-gas terms. As before, we assume spherical charge densities; the method is readily adapted to nonspherical charge distributions.

We start by writing the total charge density, including the nuclei, as

$$\rho_T(\vec{x}) = \sum_i \sum_{\vec{l}} Z_i \delta(\vec{x} - \vec{r}_{il}) - \rho_i(\vec{x} - \vec{r}_{il}) \ ,$$

where Z_i is the nuclear charge and $\delta(\vec{x})$ is the Dirac delta function. The electrostatic interaction energy may be written as the difference between the total electrostatic energy per unit cell and the electrostatic self-energies of the charge distributions in a unit cell. The total energy per unit cell is given by

$$W_T = \tfrac{1}{2} \int_V dx \rho_T(\vec{x}) \Phi_T(\vec{x}) \ ,$$

where

$$\Phi_T(\vec{x}) = \int d\vec{y} \rho_T(\vec{y}) / |\vec{x} - \vec{y}|$$

is the electrostatic potential due to $\rho_T(\vec{y})$. From the periodicity of $\Phi_T(\vec{x})$, it follows that W_T may also be written as

$$W_T = \tfrac{1}{2} \int d\vec{x} \sum [Z_i \delta(\vec{x} - \vec{r}_i) - \rho_i(\vec{x} - \vec{r}_i)] \Phi_T(\vec{x}) \ , \tag{6}$$

where we integrate over all space and sum over a single unit cell.

The electrostatic interaction energy is obtained by subtracting the self-energy terms from Eq. (6) which yields

$$W_E = \tfrac{1}{2} \int d\vec{x} \sum_i \{ [Z_i \delta(\vec{x} - \vec{r}_i) - \rho_i(\vec{x} - \vec{r}_i)] \Phi_i(\vec{x}) \} \ , \tag{7}$$

where

$$\Phi_i(\vec{x}) = \int d\vec{y} [\rho_T(\vec{y}) - Z_i \delta(\vec{y} - \vec{r}_i) + \rho_i(\vec{y} - \vec{r}_i)] / |\vec{x} - \vec{y}| \ . \tag{8}$$

If Q_i is the number of electrons in the distribution $\rho_i(\vec{x})$ such that

$$Q_i = \int d\vec{x}\rho_i(\vec{x}-\vec{r}_i) \tag{9}$$

and

$$N_i = Z_i - Q_i \tag{10}$$

is the net ionic charge on a distribution, the interaction energy can be split into four terms:

$$W_M = \tfrac{1}{2}\int d\vec{x}\int d\vec{y}\sum_i N_i\delta(\vec{x}-\vec{r}_i)\left[\sum_j\sum_{\vec{l}}{}' N_j\frac{\delta(\vec{y}-\vec{r}_{jl})}{|\vec{x}-\vec{y}|}\right], \tag{11}$$

$$W_1 = \tfrac{1}{2}\int d\vec{x}\int d\vec{y}\sum_i\sum_j\sum_{\vec{l}}{}' N_i\delta(\vec{x}-\vec{r}_i)\frac{[Q_j\delta(\vec{y}-\vec{r}_{jl})-\rho_j(\vec{y}-\vec{r}_{jl})]}{|\vec{x}-\vec{y}|}, \tag{12}$$

$$W_2 = \tfrac{1}{2}\int d\vec{x}\int d\vec{y}\sum_i\sum_j\sum_{\vec{l}}{}' [Q_i\delta(\vec{x}-\vec{r}_i)-\rho_i(\vec{x}-\vec{r}_i)]\frac{N_j\delta(\vec{y}-\vec{r}_{jl})}{|\vec{x}-\vec{y}|}, \tag{13}$$

$$W_3 = \tfrac{1}{2}\int d\vec{x}\int d\vec{y}\sum_i[Q_i\delta(\vec{x}-\vec{r}_i)-\rho_i(\vec{x}-\vec{r}_i)]\left\{\sum_j\sum_{\vec{l}}{}'\frac{[Q_j\delta(\vec{y}-\vec{r}_{jl})-\rho_j(\vec{y}-\vec{r}_{jl})]}{|\vec{x}-\vec{y}|}\right\}. \tag{14}$$

The prime on the lattice sum in these expressions indicates that the vector $\vec{r}_l = 0$ is excluded if $i = j$.

It is easy to see that Eq. (11) integrates to

$$W_M = \tfrac{1}{2}\sum_i\sum_j\sum_{\vec{l}}{}'\frac{N_iN_j}{|\vec{r}_i-\vec{r}_{jl}|} \tag{15}$$

and is equal to the Madelung energy of the crystal. It may be calculated by a variety of techniques[2] such as the Ewald double sum formula.[15]

Let us now define

$$I_j(\vec{x}) = \int d\vec{y}\frac{\rho_j(\vec{y})}{|\vec{x}-\vec{y}|} \tag{16}$$

to be the electrostatic potential of the electron distribution $\rho_j(\vec{y})$. It then follows that Eq. (12) may be written as

$$W_1 = \tfrac{1}{2}\sum_i\sum_j\sum_{\vec{l}}{}' N_i\left[\frac{Q_j}{|\vec{r}_i-\vec{r}_{jl}|} - I_j(\vec{r}_i-\vec{r}_{jl})\right]. \tag{17}$$

This term gives the interaction of the monopole moments in the unit cell with the nonpoint Coulomb part of the lattice potential.

We can show that the term W_2, which gives the interaction energy of the nonpoint Coulomb part of the charge distributions in the unit cell with the point Coulomb part of the lattice potential, is identical to W_1. Integrating Eq. (13) over $\vec{x}$, we find

$$W_2 = \tfrac{1}{2}\int d\vec{y}\sum_i\sum_j\sum_{\vec{l}}{}' N_j\delta(\vec{y}-\vec{r}_{jl})\left[\frac{Q_i}{|\vec{y}-\vec{r}_i|} - I_i(\vec{y}-\vec{r}_i)\right]. \tag{18}$$

This is shown to be equal to Eq. (17) by first integrating over $\vec{y}$, then switching indices on the summations over i and j, and finally changing the lattice summation from $+\vec{l}$ to $-\vec{l}$.

The terms W_1 and W_2 are calculated by performing a simple lattice summation of the nonpoint Coulomb potential at each nuclear site in the unit cell. Since the nonpoint Coulomb part of the potential of a spherically symmetric distribution falls off rapidly with distance, these sums are rapidly convergent.

The remaining term to be calculated, W_3, arises from the overlap of the charge distributions and is more difficult to evaluate than the other terms. It could be expanded and written as a sum of pair contributions, and for many charge distributions each pair interaction could be calculated analytically. In practice, however, there is little advantage in using this approach, and it is easier to evaluate this term numerically. Since the electron-gas terms are to be calculated by numerical integration, the most efficient method for calculating this overlap term would be to combine it with the evaluation of the other terms. As it is now written, however, Eq. (14) is poorly suited for multidimensional quadrature; the integrand is singular at the nuclear positions. We can derive an expression which is easily integrated numerically at the expense of introducing two additional lattice summations. It will be seen, however, that the additional terms add negligibly to the computational effort.

In order to bring Eq. (14) into a more tractable form we will make use of techniques similar to those employed by Bertaut[16] for the calculation of the Madelung energy. Consider a lattice of normalized spherically symmetric charge distributions, $\sigma_j(\vec{y})$, of arbitrary functional form. The total charge density in the lattice will be

$$\rho'(\vec{y}) = \sum_j\sum_{\vec{l}} Q_j\sigma_j(\vec{y}-\vec{r}_{jl}). \tag{19}$$

After adding and subtracting this density from the integral over $\vec{y}$ in Eq. (14), we split the result into four terms such that

$$W_3 = W_4 + W_S + W_0 - W_R \ ,$$

where

$$W_4 = \tfrac{1}{2}\int d\vec{x}\int d\vec{y}\sum_i\sum_j\sum_{\vec{l}}{}'\,[Q_i\delta(\vec{x}-\vec{r}_i)-\rho_i(\vec{x}-\vec{r}_i)]\frac{Q_j\delta(\vec{y}-\vec{r}_{jl})}{|\vec{x}-\vec{y}|} \ , \tag{20}$$

$$W_S = \tfrac{1}{2}\int d\vec{x}\sum_i[Q_i\delta(\vec{x}-\vec{r}_i)-\rho_i(\vec{x}-\vec{r}_i)]\int d\vec{y}\frac{Q_i\sigma_i(\vec{y}-\vec{r}_i)}{|\vec{x}-\vec{y}|} \ , \tag{21}$$

$$W_0 = \tfrac{1}{2}\int d\vec{x}\sum_i\left[[Q_i\delta(\vec{x}-\vec{r}_i)-\rho_i(\vec{x}-\vec{r}_i)]\int d\vec{y}\left(\sum_j\sum_{\vec{l}}{}'\,Q_j\sigma_j(\vec{y}-\vec{r}_{jl})-\rho_j(\vec{y}-\vec{r}_{jl})\right)\Big/|\vec{x}-\vec{y}|\right] \ , \tag{22}$$

$$W_R = \tfrac{1}{2}\int d\vec{x}\sum_i[Q_i\delta(\vec{x}-\vec{r}_i)-\rho_i(\vec{x}-\vec{r}_i)]\int d\vec{y}\frac{\rho'(\vec{y})}{|\vec{x}-\vec{y}|} \ . \tag{23}$$

Since W_4 has the same basic form as W_2, Eq. (13), it follows immediately from Eqs. (17) and (18) that

$$W_4 = \tfrac{1}{2}\sum_i\sum_j\sum_{\vec{l}}{}'\,Q_i\left(\frac{Q_j}{|\vec{r}_i-\vec{r}_{jl}|}-I_j(\vec{r}_i-\vec{r}_{jl})\right) \ .$$

This term may then be combined with Eqs. (17) and (18) to get a new term

$$W_D = \tfrac{1}{2}\sum_i\sum_j\sum_{\vec{l}}{}'\,(Z_i+N_i)\left(\frac{Q_j}{|\vec{r}_i-\vec{r}_{jl}|}-I_j(\vec{r}_i-\vec{r}_{jl})\right) \ , \tag{24}$$

which is easily calculated as a rapidly convergent, direct lattice summation of the nonpoint Coulomb potential at each nuclear site in the unit cell.

Next we define

$$H_j(\vec{x}) = \int d\vec{y}\,\sigma_j(\vec{y})/|\vec{x}-\vec{y}| \tag{25}$$

to be the electrostatic potential of the charge distribution $\sigma_j(\vec{y})$. Then after integrating over the delta function in Eq. (21) we have

$$W_S = \tfrac{1}{2}\sum_i\left(Q_i^2H_i(0)-\int d\vec{x}Q_i\rho_i(\vec{x}-\vec{r}_i)H_i(\vec{x}-\vec{r}_i)\right) \ .$$

This can be combined into a single integration by substituting Eq. (9) for Q_i, and changing variables in the second integration to get

$$W_S = \tfrac{1}{2}\sum\int d\vec{x}\rho_i(\vec{x})Q_i[H_i(0)-H_i(\vec{x})] \ . \tag{26}$$

To evaluate this expression, we must calculate one center integrals for each different charge distribution, which depend only upon the $\rho_i(\vec{x})$ and $\sigma_i(\vec{y})$ chosen. They are independent of the lattice geometry and will not affect the position of the energy minimum. Thus they need only be calculated once in the entire energy minimization.

The term that will be calculated numerically is W_0, Eq. (22). This can be written as

$$W_0 = \tfrac{1}{2}\int d\vec{x}\sum_i[Q_i\delta(\vec{x}-\vec{r}_i)-\rho_i(\vec{x}-\vec{r}_i)]\sum_j\sum_{\vec{l}}{}'\,[Q_jH_j(\vec{x}-\vec{r}_{jl})-I_j(\vec{x}-\vec{r}_{jl})] \ ,$$

where Eqs. (25) and (16) have been used. An integration over the delta function and the substitution of Eq. (9) then yields

$$W_0 = \tfrac{1}{2}\int d\vec{x}\sum_i\rho_i(\vec{x}-\vec{r}_i)[\Phi_0(\vec{r}_i)-\Phi_0(\vec{x})-P_i(0)+P_i(\vec{x}-\vec{r}_i)] \ ,$$

where we have defined

$$\Phi_0(\vec{x}) = \sum_j\sum_{\vec{l}}{}'P_j(\vec{x}-\vec{r}_{jl}) \tag{27}$$

and

$$P_j(\vec{x}) = Q_jH_j(\vec{x})-I_j(\vec{x}) \ . \tag{28}$$

As will be seen below, this term is relatively easy to integrate numerically. In order to calculate it with the electron-gas terms, the integration over space must be transformed into an integration over a unit cell. Thus we break up

the integration over space into a sum of the form

$$W_0=\tfrac{1}{2}\sum_{\vec{l}}\int_{V_l}d\vec{x}'\sum_i\rho_i(\vec{x}'-\vec{r}_i)[\Phi_0(\vec{r}_i)-\Phi_0(\vec{x}')-P_i(0)+P_i(\vec{x}'-\vec{r}_i)]\ .$$

This is then followed by a change of variables to $\vec{x}=\vec{x}'-\vec{r}_l$, which allows the interchange of the order of lattice summation and integration. Finally we make use of the periodicity of $\Phi_0(\vec{x})$, Eq. (27), and convert the lattice sum to one over $-\vec{l}$ to get

$$W_0=\tfrac{1}{2}\int_V d\vec{x}\sum_i\sum_{\vec{l}}\rho_i(\vec{x}-\vec{r}_{il})[\Phi_0(\vec{r}_i)-\Phi_0(\vec{x})-P_i(0)+P_i(\vec{x}-\vec{r}_{il})]\ . \tag{29}$$

In this form W_0 is ideally suited for integration with the electron-gas terms. It should be clear that for $\vec{x}$ near a nucleus, where the density is sharply peaked, the potential term in square brackets is very small. In addition, since the choice of the $\sigma_j(y)$ is arbitrary, an appropriate choice of these functions screens the electronic potentials and makes $\Phi_0(x)$ and the $P_j(\vec{x})$ smooth and small. This ensures that the convergence of this term is no worse than that of the electron-gas terms.

Next, we develop an expression for the remaining term, W_R, Eq. (23). This term is conveniently calculated as a series in the reciprocal lattice of the crystal. This series will be seen to converge rapidly provided some easily satisfied constraints on the $\sigma_j(\vec{y})$ are imposed.

Since $\rho'(\vec{x})$, Eq. (19), is periodic, it can be expanded as a Fourier series in the reciprocal lattice

$$\rho'(\vec{y})=V^{-1}\sum_{\vec{k}}C(\vec{k})e^{-i\vec{k}\cdot\vec{y}}\ , \tag{30}$$

where V is the volume per unit cell and the sum extends over all reciprocal-lattice vectors $\vec{k}$. The expansion coefficients are given by

$$\begin{aligned}C(\vec{k})&=\int_V d\vec{y}e^{i\vec{k}\cdot\vec{y}}\sum_j\sum_{\vec{l}}Q_j\sigma_j(\vec{y}-\vec{r}_{jl})\\&=\sum_j e^{i\vec{k}\cdot\vec{r}_j}\int d\vec{y}e^{i\vec{k}\cdot\vec{y}}\sigma_j(\vec{y})\ ,\end{aligned} \tag{31}$$

where the lattice summation and integration over a single unit cell have been converted by a change of variables to an integration over all space. We can integrate over the delta function in Eq. (23) and again use Eq. (9). When Eq. (30) is then substituted into the resulting expression and the $\vec{k}=0$ term is separated from the remainder of the sum, we have

$$W_R=W_R'+W_R''\ , \tag{32}$$

where

$$W_R'=(2V)^{-1}C(0)\int d\vec{x}\int d\vec{y}\sum_i\rho_i(\vec{x}-\vec{r}_i)\left(\frac{1}{|\vec{r}_i-\vec{y}|}-\frac{1}{|\vec{x}-\vec{y}|}\right) \tag{33}$$

and

$$W_R''=(2V)^{-1}\sum_{\vec{k}}{}'C(\vec{k})\int d\vec{x}\int d\vec{y}\sum_i\rho_i(\vec{x}-\vec{r}_i)e^{-i\vec{k}\cdot\vec{y}}\left(\frac{1}{|\vec{r}_i-\vec{y}|}-\frac{1}{|\vec{x}-\vec{y}|}\right)\ . \tag{34}$$

The prime on the reciprocal-lattice summation indicates that the term $\vec{k}=0$ is excluded from the sum. A straightforward integration over $\vec{y}$ reduces Eq. (33) to

$$W_R'=2\pi V^{-1}C(0)\int d\vec{x}\,x^2\frac{\rho_i(\vec{x})}{6}\ . \tag{35}$$

The integrals over $\vec{y}$ in Eq. (34) may be evaluated using the identity

$$\int d\vec{y}\,e^{-i\vec{k}\cdot\vec{y}}/|\vec{z}-\vec{y}|=4\pi e^{-i\vec{k}\cdot\vec{z}}/k^2\ .$$

This yields

$$W_R''=2\pi V^{-1}\sum_{\vec{k}}{}'C(\vec{k})\sum_i e^{-i\vec{k}\cdot\vec{r}_i}\int d\vec{x}\,\rho_i(\vec{x})\frac{(1-e^{-i\vec{k}\cdot\vec{x}})}{k^2}\ .$$

For spherically symmetric charge distributions it is not necessary to evaluate W_R' and W_R'' separately, since W_R' is identical to the $\vec{k}=0$ term in the series

$$W_R=2\pi V^{-1}\sum_{\vec{k}}C(\vec{k})\sum_i e^{-i\vec{k}\cdot\vec{r}_i}\phi_i^*(k)\ , \tag{36}$$

where

$$\phi_i(k)=\int d\vec{x}\,\rho_i(\vec{x})(1-e^{i\vec{k}\cdot\vec{x}})/k^2\ . \tag{37}$$

This assertion can be verified by examining the limiting behavior of Eq. (37) as $|\vec{k}|$ approaches zero and comparing the result to Eq. (35) for spherically symmetric $\rho_j(\vec{x})$.

For actual atomic charge distributions, the discontinuous first derivative of the density at the nucleus

causes $\phi_i(\vec{k})$ to fall off slowly with distance in the reciprocal space. This presents no difficulty, however, since the $C(\vec{k})$ in Eq. (37) will converge as the Fourier transform of the $\sigma_j(\vec{y})$. We can guarantee that W_R converges exponentially by choosing the $\sigma_j(\vec{y})$ as Gaussian functions or linear combinations of Gaussians. For the crystal structures calculated here we have found that a single Gaussian

$$\sigma_j(\vec{y}) = (\alpha_j^2/\pi)^{3/2} \exp(-\alpha_j^2 y^2) \tag{38}$$

gives acceptable convergence of the overlap term Eq. (29) and, at the same time, allows rapid convergence of the reciprocal-lattice summation.

The efficiency of the calculation is further improved by combining the calculation of W_R with the evaluation of the Madelung energy, Eq. (14). In the Appendix we generalize the Ewald double sum formula[15] to the case of a lattice of Gaussians of different halfwidths. The Madelung energy may then be calculated as

$$W_M = 2\pi V^{-1} \sum_{\vec{k}}{}' F(\vec{k}) B(-\vec{k}) \Big/ k^2 + \tfrac{1}{2} \sum_i \sum_j \sum_{\vec{l}}{}' N_i N_j \left(\frac{1}{|\vec{r}_i - \vec{r}_{jl}|} - H_j(\vec{r}_i - \vec{r}_{jl}) \right) - \sum_i N_i^2 H_i(0) \ , \tag{39}$$

where

$$F(\vec{k}) = \sum_i N_i e^{i\vec{k}\cdot\vec{r}_i} \tag{40}$$

and

$$B(\vec{k}) = \sum_j N_j e^{i\vec{k}\cdot\vec{r}_j} \int d\vec{y}\, e^{i\vec{k}\cdot\vec{y}} \sigma_j(\vec{y}) \ . \tag{41}$$

III. NUMERICAL METHODS

In the calculation of the binding energy, the energy terms which require the greatest computational effort are the electron-gas terms and the electrostatic overlap term, which are evaluated by a three-dimensional numerical integration. This is a time consuming operation because at each integration point a lattice summation of the density and the screened potentials $P_j(\vec{x} - \vec{r}_{il})$ is required. The integrand is evaluated more quickly if cubic spline interpolation is used to find the cube root of the densities and the potentials. A significant savings in computer time is also gained by interpolating the quantities $\phi(k)$, which appear in the reciprocal-lattice summation.

For a given lattice geometry, an efficient evaluation of the energy results from the choice of a quadrature technique which requires relatively few integration points. Test calculations on alkali halide crystals revealed that the integrand of the kinetic energy term, Eqs. (4a) and (5), increases by several orders of magnitude within a small sphere surrounding each nucleus where the charge density is very sharply peaked. These spherical regions typically account for 5% of the total value of the integral. Similar behavior was observed in the integrands of the exchange and overlap terms, but to a lesser extent. In this case, standard multidimensional integration techniques,[17,18] would give unreliable results unless an excessively large number of integration points was used. Thus an efficient quadrature scheme must pay special attention to the regions around each nucleus.

Since the peaking of the kinetic and exchange terms is obviously due to the behavior of the density, convergence of the numerical integration can be improved by forcing the density to be smooth within a small sphere around each nucleus. The error introduced in this step can be corrected for in a separate integration. To make this clearer, suppose that W is either the kinetic or exchange energy. From Eqs. (4a), (4b), and (5) we see that both terms may be written as

$$W = \int_V d\vec{x}' J(\vec{x}') \ , \tag{42}$$

where $J(x')$ has the form

$$J(\vec{x}') = C \left[\left(\sum_j \sum_{\vec{l}} \rho_j(\vec{x}' - \vec{r}_{jl}) \right)^n - \sum_j \sum_{\vec{l}} [\rho_j(\vec{x}' - \vec{r}_{jl})]^n \right] \ , \tag{43}$$

with $n = \frac{5}{3}$ or $n = \frac{4}{3}$. We write this as a three-dimensional integration of an approximate integrand which is smoother than $J(\vec{x}')$, plus some correction terms to be determined later. Thus we define

$$W = W' + \sum_i W_i \ , \tag{44}$$

where

$$W' = \int_V d\vec{x}\, J'(\vec{x}) \ .$$

The W_i are the corrections to the quadrature over a unit cell of the approximate integrand $J'(\vec{x})$. In $J'(x)$ we use the altered densities

$$\rho_i'(r) = \begin{cases} \rho_i(r), & r \geq \delta_i \\ (a_i + b_i r^2)^3, & r < \delta_i, \end{cases} \tag{45}$$

with $r = |\vec{x} - \vec{r}_{il}|$. The parameters a_i and b_i are fixed by requiring continuity of the density $\rho_i(r)$ and its first derivative at δ_i. Whereas the correct $J(\vec{x})$, Eq. (43), has large peaks and a discontinuous first derivative at the nucleus, $J'(x)$, calculated using Eq. (45),

is relatively flat and has continuous first derivatives everywhere. As will be shown below, this gives remarkably improved convergence of the integrations.

The W_i in Eq. (44) are determined by integrating the difference between the actual and approximate integrands within the small spherical region of radius δ_i about each nucleus. It is possible to derive an expression for the W_i that is easy to calculate and yet holds to a high accuracy.

Consider the integrand of Eq. (42) after a change of variables to $\vec{x}=\vec{x}'-\vec{r}_i$. Let

$$f_i(\vec{x}) = \sum_j \sum_{\vec{l}}{}' \frac{\rho_j(\vec{x}+\vec{r}_i-\vec{r}_{jl})}{\rho_i(\vec{x})}$$

and separate the density of the charge distribution centered at $\vec{x}=0$ from the others in $J(\vec{x}+\vec{r}_i)$. This gives

$$J(\vec{x}+\vec{r}_i) = C\Bigg\{[\rho_i(\vec{x})]^n[1+f_i(\vec{x})]^n - [\rho_i(\vec{x})]^n - \sum_j \sum_{\vec{l}}{}' [\rho_j(\vec{x}+\vec{r}_i-\vec{r}_{jl})]^n\Bigg\} .$$

Within a small sphere around the nucleus $f_i(\vec{x}) << 1$, and the above expression may be expanded by the binomial theorem to obtain

$$J(\vec{x}+\vec{r}_i) = C\Bigg\{[\rho_i(\vec{x})]^n\Big[nf_i(\vec{x}) + \tfrac{1}{2}n(n-1)f_i^2(x)+\cdots\Big] - \sum_j \sum_{\vec{l}}{}' [\rho_j(\vec{x}+\vec{r}_i-\vec{r}_{jl})]^n\Bigg\} .$$

It is clear that the leading term is much larger than the rest, so that

$$J(\vec{x}+\vec{r}_i) \approx nC\Bigg(\sum_j \sum_{\vec{l}}{}' \rho_j(\vec{x}+\vec{r}_i-\vec{r}_{jl})\Bigg)[\rho_j(\vec{x})]^{n-1} .$$

The correction terms in Eq. (3) are then approximated as

$$W_i = nC\int_{S_i} d\vec{x}\Bigg(\sum_j \sum_{\vec{l}}{}' \rho_j(\vec{x}+\vec{r}_i-\vec{r}_{jl})\Bigg) \times \{[\rho_i(\vec{x})]^{n-1}-[\rho_i'(\vec{x})]^{n-1}\} , \quad (46)$$

where we integrate over the small sphere of radius δ_i centered at $\vec{r}_i$.

The above expression lends itself to a further approximation since the first term in square brackets is much more slowly varying than the other factor in the integrand. The spherically symmetric densities in this term may be expanded in a Taylor series about $\vec{r}_i$ to obtain

$$\rho_j(\vec{x}+\vec{r}_i-\vec{r}_{jl}) = \rho_j(\vec{r}_i-\vec{r}_{jl}) + [|\vec{x}+\vec{r}_i-\vec{r}_{jl}|-|\vec{r}_i-\vec{r}_{jl}|]\frac{d\rho_j}{dr}\bigg|_{r=|\vec{r}_i-\vec{r}_{jl}|} + \cdots .$$

Then since for small $|\vec{x}|$

$$|\vec{x}+\vec{r}_i-\vec{r}_{jl}| \approx |\vec{r}_i-\vec{r}_{jl}|[1+\vec{x}\cdot(\vec{r}_i-\vec{r}_{jl})/(\vec{r}_i-\vec{r}_{jl})^2] ,$$

we have

$$\rho_j(\vec{x}+\vec{r}_i-\vec{r}_{jl}) \approx \rho_j(\vec{r}_i-\vec{r}_{jl}) + \left(\frac{\vec{x}\cdot(\vec{r}_i-\vec{r}_{jl})}{|\vec{r}_i-\vec{r}_{jl}|}\right)\frac{d\rho_j}{dr}\bigg|_{r=|\vec{r}_i-\vec{r}_{jl}|} . \quad (47)$$

When this term is substituted into Eq. (46) and the angular integrations are carried out, all terms depending upon the derivatives of the density vanish and there remains

$$W_i = 4\pi nC\Bigg(\sum_j \sum_{\vec{l}}{}' \rho_j(\vec{r}_i-\vec{r}_{jl})\Bigg)\int_0^{\delta_i} dx\, x^2\{[\rho_i(x)]^{n-1}-[\rho_i'(x)]^{n-1}\} . \quad (48)$$

Note that the expression to be integrated here involves a one-dimensional quadrature that does not depend upon the lattice geometry. The integral in Eq. (48) need only be calculated at the start of an energy minimization, and each W_i is then relatively simple to calculate as the geometry of the lattice is varied.

As was noted earlier, convergence difficulties also appear in the direct numerical integration of the electrostatic overlap term. This is due to the peaked nature of the screened potentials, $P_i(\vec{x})$, in the vicinity of a nucleus, which is in turn a result of the differences between Gaussian and actual charge densities close to the origin. The problem may be alleviated by choosing large exponential parameters for the Gaussians, but then the reciprocal-lattice summations

will be slowly convergent. Fortunately, it is possible to avoid these difficulties with an approach similar to that used for the kinetic and exchange terms.

The electrostatic overlap term can be approximated by replacing the actual charge densities with those of Eq. (45), and the actual screened potentials by

$$P_i'(r)=\begin{cases}P_i(r), & r\geq\delta_i\\ c_i+d_i r^2, & r<\delta_i;\end{cases} \tag{49}$$

where c_i and d_i are determined by requiring continuity of $P_i'(r)$ and its first derivative at $r=\delta_i$. This makes the approximate integrand of W_0 smooth and well behaved.

The errors introduced into the overlap integration can be corrected for in much the same way as for the kinetic and exchange terms. By examining the integrand of W_0, it can be shown that the correction term to be added for each nucleus is of the form

$$W_i=\tfrac{1}{2}\int_{S_i}d\vec{x}\left[\left(\sum_j\sum_{\vec{l}}{}'P_j(\vec{r}_i-\vec{r}_{jl})-P_j(\vec{x}+\vec{r}_i-\vec{r}_{jl})\right)[\rho_i(\vec{x})-\rho_i'(x)]-\left(\sum_j\sum_{\vec{l}}{}'\rho_j(\vec{x}+\vec{r}_i-\vec{r}_{jl})\right)[P_i(\vec{x})-P_i'(\vec{x})]\right] .$$

This expression is simplified considerably by expanding both the $P_j(\vec{x}+\vec{r}_i-\vec{r}_{jl})$ and $\rho_j(\vec{x}+\vec{r}_i-\vec{r}_{jl})$ in Taylor series about $\vec{r}_i$. The leading terms in the expansion of the $P_j(\vec{x}+\vec{r}_i-\vec{r}_{jl})$ cancels with the constant term and after integrating over angles we are left with

$$W_i=2\pi\left(\sum_j\sum_{\vec{l}}{}'\rho_j(\vec{r}_i-\vec{r}_{jl})\right)\int_0^{\delta_i}dx\,x^2[P_i(x)-P_i'(x)] . \tag{50}$$

As was the case with the exchange and kinetic energy terms, the part to be integrated here is independent of the lattice geometry.

For the three-dimensional quadratures of the approximate integrands we have obtained very satisfactory results using the method of Conroy[18] and a total of 1154 integration points in the unit cell. In Table I we give the results of a number of trial calculations for the NaF crystal. Since the energy is invariant to a

TABLE I. Contributing terms to the binding energy in NaF. The results for all trials except trial 12 are based on a primitive rhombohedral unit cell with $\alpha=60°$ and $a=6.3498$ a.u. All energies are given in a.u. (1 a.u. = 627.5 kcal/mole).

Trial	Total W_B [Eq. (1)]	Exchange $W_X(10^{-1})$	Kinetic $W_K(10^{-1})$	Correlation $W_C(10^{-1})$	Overlap $W_O(10^{-1})$	Nonpoint Coulomb electrostatic $(W_E-W_M)(10^{-1})$	Net short range $(W_B-W_M)(10^{-1})$	Key
1	−0.314 27	−0.282 25	1.161 26	−0.023 458	0.203 59	−0.106 05	0.749 46	a,b,c
2	−0.353 32	−0.276 81	0.771 21	−0.023 460	0.191 60	−0.112 046	0.358 89	a,d,c
3	−0.353 02	−0.276 97	0.774 39	−0.023 458	0.191 57	−0.112 05	0.361 89	a,e,c
4	−0.352 23	−0.277 13	0.781 92	−0.023 463	0.192 68	−0.111 50	0.369 82	f,b,c
5	−0.352 20	−0.277 13	0.781 92	−0.023 462	0.192 87	−0.111 41	0.370 05	f,g,c
6	−0.352 18	−0.277 16	0.782 32	−0.023 456	0.192 86	−0.111 41	0.370 28	f,e,c
7	−0.352 17	−0.277 14	0.782 37	−0.023 461	0.192 98	−0.111 36	0.370 41	f,h,c
8	−0.352 20	−0.277 13	0.782 01	−0.023 461	0.193 20	−0.111 25	0.370 17	i,h,c
9	−0.352 20	−0.277 13	0.782 16	−0.023 459	0.192 73	−0.111 48	0.370 09	j,h,c
10	−0.352 15	−0.277 14	0.782 37	−0.023 460	0.056 575	−0.111 17	0.370 60	f,h,k
11	−0.352 45	−0.277 14	0.782 37	−0.023 460	2.235 58	−0.114 19	0.367 57	f,h,l
12	−0.352 28	−0.277 14	0.782 01	−0.023 465	0.191 47	−0.112 11	0.369 28	f,m,c

[a]Calculated using exact densities and screened potentials.
[b]Nuclei shifted by $(0.4766\times10^{-3},\ 0.159\,879,\ 0.246\,534)$ from positions in h.
[c]Exponential parameters for Gaussian functions (see text) are $\alpha_{Na^+}=1.0$ a.u.$^{-1}$ and $\alpha_{F^-}=0.7$ a.u.$^{-1}$.
[d]Nuclei shifted by (0.111 99, 0.079 879, 0.240 47) from positions in h.
[e]Nuclei shifted by (0.011, 0.022, 0.033) from positions in h.
[f]Calculated using Eqs. (45) and (49) with $\delta_{Na^+}=0.4$ a.u. and $\delta_{F^-}=0.4$ a.u.
[g]Nuclei shifted by $(0.476\,57\times10^{-3},\ 0.159\,88,\ 0.2265)$ from positions in h.
[h]Na^+ nucleus located at (0,0,0) and F^- nucleus located at $(\frac{1}{2},\frac{1}{2},\frac{1}{2})$ with respect to primitive unit-cell axes.
[i]Calculated using Eqs. (45) and (49) with $\delta_{Na^+}=0.3$ a.u. and $\delta_{F^-}=0.3$ a.u.
[j]Calculated using Eqs. (45) and (49) with $\delta_{Na^+}=0.5$ a.u. and $\delta_{F^-}=0.5$ a.u.
[k]Exponential parameters changed to $\alpha_{Na^+}=1.2$ a.u.$^{-1}$ and $\alpha_{F^-}=0.9$ a.u.$^{-1}$.
[l]Exponential parameters changed to $\alpha_{Na^+}=0.8$ a.u.$^{-1}$ and $\alpha_{F^-}=0.5$ a.u.$^{-1}$.
[m]Calculated using conventional cubic unit cell with $a=\sqrt{2}(6.3498)$ a.u.

uniform translation of all the ions in the unit cell, the convergence of the integrals can be checked by shifting the origin of the unit cell with respect to the ions, leaving all other geometrical parameters fixed. A large number of pseudorandom shifts can be generated by attempting to minimize the energy with respect to the origin of the unit cell. This is the procedure followed in the first six trials in Table I, and we report the maximum changes in the energy discovered in the minimization attempts. In the first three trials in Table I, the exact densities and screened potentials were used, while in the remaining trials the approximate functions, Eqs. (45) and (49), were used. In the first and fourth trials both the Na^+ and F^- nuclei have been displaced from their conventional positions at (0,0,0) and $(\frac{1}{2},\frac{1}{2},\frac{1}{2})$, such that the Na^+ nucleus coincides with one of the integration points. The peaked nature of the exact kinetic energy integrand is revealed when the first trial is compared to the second and third, where no integration points fell close to the nucleus. The kinetic energy term, W_K, is about 0.04 a.u. higher in the first case than in the next two cases, and the binding energy is significantly changed by this error. The convergence of the exchange term, W_X, and the overlap term, W_O, is better but still not satisfactory. Due to the partial cancellation of these terms, the total short-range energy, $W_B - W_M$, in the first trial is about twice the actual value, while in the next two trials it is about 0.001 a.u. too low.

The use of Eqs. (45) and (49) and the correction terms in trials 4 through 7 improves the convergence dramatically. All of the terms agree to within at least three significant figures and binding energy W_B is accurate to four. This is more than sufficient to ensure that the energy minimum can be found to within the accuracy of the electron-gas theory.

Obviously, the results of this quadrature scheme will only be meaningful if they do not significantly depend upon the choice of the parameters δ_j and α_j. In trials 8 through 11 these parameters were varied from the values used in the previous trials, and the agreement of the various terms is excellent. The results of trials 8 and 9 show that the results do not critically depend upon choice of the radius δ_j and the results of trials 10 and 11 show that the nonpoint Coulomb electrostatic energy $W_E - W_M$ is not terribly sensitive to the choice of α_j. In trial 11, however, the chosen Gaussian parameters are too small and fail to adequately shield the actual electrostatic potential of the electron distributions. It is best to adjust the α_j so that the overlap term, W_0, is of the same order of magnitude as the kinetic and exchange term.

As a final test of the numerical method, in trial 12 we optimized the NaF structure based on the conventional cubic unit cell which contains four formula units. The results are essentially the same as the results of the energy minimization in trial 7, and show that the integration with 1154 points can be used for much larger unit cells than the primitive NaF cell. Further tests on systems with larger unit cells revealed that 1154 integration points are insufficient to guarantee convergence of the short-range energy when there are ten or more atoms in the unit cell. For the larger unit cells these errors do not appear to result from the behavior of the integrand near the nuclei. Thus the integrations require about 100 points for each ion in the unit cell.

IV. IMPROVED CRYSTAL CHARGE DENSITIES

The two distinct approximations made in the electron-gas theory are that the energy can be calculated from the density functionals in Eqs. (4) and that the total density of the system can be written as a superposition of the charge densities of the separated species. Improvements to the model can be made by using more exact density functionals and by using a better description of the density in the interacting systems. For neutral closed-shell systems the superposition of the gas phase charge densities should be a very good approximation. The excellent results that have been obtained for rare-gas interactions,[6] thus make it appear that the density functionals are adequate and that attempts to improve the model for charged species should focus on describing induction effects on the charge densities.

As was discussed in the Introduction, the perturbations that occur in an atomic charge density when it is placed in the electrostatic potential of the crystal lattice are twofold. The size change effect is due to the spherically symmetric part of the potential which causes contractions and expansions of the charge distribution with no loss of spherical symmetry. Polarization effects are due to electric fields and their gradients in the lattice which distort ions from spherical symmetry. The size change effect occurs in all types of ionic crystals while polarization will only be significant in crystals of low symmetry where there are large gradients in the electrostatic potential. In this paper we will limit ourselves to size change effects only.

A simple model for calculating ionic wave functions and charge densities in crystals has been proposed by Pachalis and Weiss (PW),[19] which is based on the earlier work of Watson.[20] In this model the crystalline potential is approximated by the potential created when a charged spherical shell is placed around the ion. The potential term

$$V_i(r) = \begin{cases} -N_i/r_0, & r \leq r_0 \\ -N_i/r, & r > r_0, \end{cases} \tag{51}$$

where $-N_i$ is the charge on the shell and r_0 its radius, is then added to the Hamiltonian of the system

and the wave function and charge density of the ion are then obtained by the Hartree-Fock self-consistent-field (SCF) method. Since the crystal is electrically neutral it is physically reasonable to take the charge on the shell to be the opposite of the ionic charge and to use the radius of the shell as a variable parameter to approximate the actual crystal potential. The shell potential stabilizes the anion. It decreases the effective size of an anion and expands a cation, although the effect is much more pronounced for the anions.

We have performed our own SCF calculations using the program of Laws and co-workers,[21] modified to include matrix elements of the potential $V_i(r)$. We have repeated and duplicated Watson's[20] calculation for the O^{2-} ion with a shell charge of $+2$ and a radius of 2.66 a.u., but have been unable to obtain agreement with any of the crystal ion wave functions reported by PW and must conclude they are in error. This conclusion is confirmed when the PW results for O^{2-} at a shell radius of 2.646 a.u., using a basis set of ten orbitals, is compared with Watson's calculations obtained with a smaller basis of only seven functions. The total energy reported by PW is $-81.511\,357$ a.u. and is considerably higher than Watson's value of -81.7484 a.u.. The PW calculations with the larger basis set should have produced a total energy slightly less than Watson's result. We have further checked our calculations by determining a wave function for F^- with a $+1$ shell charge and $r_0=0.0$. This is equivalent to increasing the nuclear charge in the Hamiltonian by one and when the same basis set as that used by Clementi and Roetti[22] is employed, we obtain the same total energy and expansion coefficients as reported in Ref. 22 for Ne.

Since the inclusion of the shell potentials can have a large effect on the wave functions, it is not always appropriate to use the same basis sets in the shell stabilized calculations as used for gas phase ion calculations. To ensure that our results are at the Hartree-Fock limit we have used the same sized basis sets as used by PW and Clementi, and for each different shell potential have individually optimized the orbital exponents.

V. EQUILIBRIUM PROPERTIES AND EXPERIMENTAL THERMODYNAMIC ENERGY CYCLES

There are a variety of procedures by which the shell stabilized (SS) charge densities of the previous section may be used to calculate the equilibrium geometry and energy of a crystal. Some of these methods, as used by others, have lead to errors and results which are not directly comparable to experimental quantities, so that we must be careful in the use of the SS densities.

Let us first consider crystals with singly charged anions. The crystal charge densities can be represented by SS densities. The crystal binding energy may be calculated from these densities, either including nonlinear many-body effects as in Sec. II or in a pairwise interaction approximation.[7(b),9] In the latter method pair potentials are calculated from SS wave functions, and from lattice sums of the pair interactions, the binding energy is obtained. If the equilibrium geometry of the crystal is found by minimization of the binding energy with respect to the geometrical parameters of the crystal, then the value of W_B at the minimum refers to the interaction energy of the crystal with respect to the SS densities at infinite separation and not the free, gaseous ions. This energy cannot be found experimentally since the free SS ions do not exist.

In Fig. 1 the variation of the equilibrium binding energy in LiF with shell potential is shown. Over the range of shell potentials considered, W_B is seen to be a monotonically decreasing function, since, as the anion shrinks, the lattice continues to contract and the binding energy decreases. Thus the minimization of W_B with respect to geometry and shell potentials cannot be used to determine the equilibrium properties and W_B should not be compared to experimental energies, as has been done in a number of previous papers.[9,11,12]

A thermodynamically meaningful energy for systems containing cations and singly charged anions is the dissociation energy, D_e, of the crystal into free cations and anions, which can be measured experi-

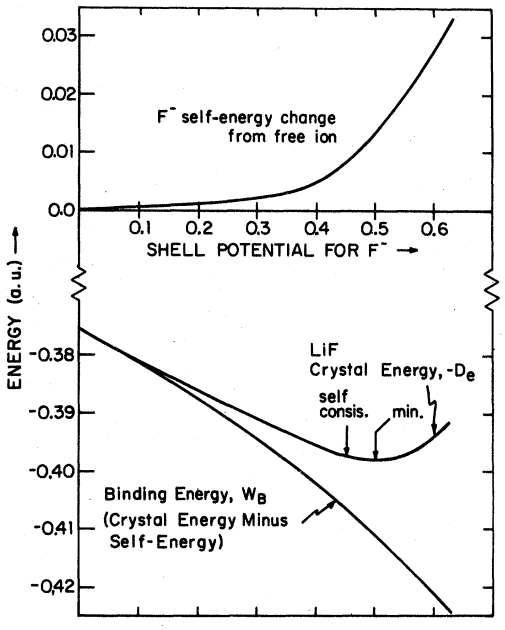

FIG. 1. Variaton of self-energy, crystal energy, and binding energy with shell potential in LiF. The self-consistent and minimum crystal energy points are indicated.

mentally for most systems. To calculate it theoretically we need to know the self-energy difference between the SS ion and the free ion. This is given by the difference between the expectation value of the free ion Hamiltonian (i.e., with the shell potential removed) with the SS wave function and the Hartree-Fock energy of the free ion. We assume[7(b)] that correlation energy differences, in this case, are negligible. The self-energy term is easily found during the SCF calculations and is plotted in Fig. 1 as a function of shell potential. It is generally a small but significant positive or destabilizing quantity which rapidly increases at high shell potentials.

The crystal energy or $-D_e$ is given by the sum of the binding energy and the self-energy change. From Fig. 1, it is seen that this quantity attains a broad minimum as a function of site potential. If the energy functionals were exact or satisfied a variational principle, the correct procedure would be to minimize $-D_e$ as a function of geometry and shell potential. Since the minimum in the crystal energy is very flat and there are errors in the energy functionals on the order of a few percent, there is no physical reason to distinguish between points close to this minimum. Instead we may choose an arbitrary but consistent criterion to pick the shell potential, provided it generally places us in the flat region of the minimum.

A simple, but physically reasonable, method of fixing the shell potential is to choose r_0 in Eq. (51) such that $V_i(r)$ matches the potential at the site of the anion nucleus. Stabilization of the cation, in a number of test cases, was found to have a negligible effect. This method of choosing anion shell potentials is easily incorporated in a self-consistent manner in the crystal energy minimization with respect to the geometrical parameters of the lattice. An initial SCF calculation can be performed with the shell potential chosen as a rough estimate of the anion site potential. The geometry is then varied to find both the minimum energy and the actual anion site potential at the minimum for this density. A new SS wave function is then calculated with r_0 chosen to match the previous site potential and the new SS density is used in the next energy minimization. Self-consistency is achieved when the shell potential of the SCF calculation matches the anion site potential at the energy minimum to within a few percent. This iterative procedure normally gives convergence of the crystal energy within the range consistent with the accuracy of the electron-gas approximation. As will be seen in the next sections, this gives excellent results, typically within 1–2% of the experimental dissociation energy and lattice parameters.

In their recent study, Mackrodt and Stewart[9] used SS wave functions to calculate equilibrium binding energies and lattice parameters in a pairwise additive approximation. The shell potential was chosen to match only the point Coulomb part of the electrostatic potential. Apparently self-energy changes of the anions were not taken into account and calculated binding energies were compared directly with experimental dissociation energies.

An additional consideration arises in the case of crystals with multiply charged anions such as O^{2-}. The oxide ion is unstable in the gas phase and its heat of formation is not an experimentally measurable quantity. Reported[11,12] values of this quantity have been obtained in part by semiempirical lattice energy calculations and actually refer to the crystalline (i.e., stabilized) O^{2-} ion in a series of crystals. Since the degree of stabilization varies from crystal to crystal, it is meaningless to report "experimental" heats of formation of the O^{2-} ion. As was discussed in Ref. 7(b), the experimentally accessible quantity is the dissociation energy of oxide crystals into cations, singly charged O^- ions, and free electrons. This quantity can be compared to purely theoretical energies. To the equilibrium binding energy of the crystal, obtained with a self-consistent SS density, we add the difference between the self-energies of the gas phase O^- ion and the SS O^{2-} ion in the absence of the shell potential. Since the number of electrons changes between the two species, it is necessary to consider correlation as well as Hartree-Fock energy differences. Until atomic correlation energies are more accurately known, we assume the correlation energy to be the same in all the SS oxide wave functions and take the correlation energy difference between O^- (^2P) and stabilized O^{2-} (^1S) to be 0.083 a.u.[7(b),23]

VI. RESULTS FOR LiF, NaF, MgO, AND CaO

The equilibrium geometries and dissociation energies of LiF, NaF, MgO, and CaO have been calculated from the pairwise MEG theory by Cohen and Gordon. In order to examine the effects of many-body forces and the SS densities on the equilibrium properties of crystals, we have applied the model presented here to these systems. First let us consider the face-centered-cubic ($B1$) phases of these crystals.

A. Properties of the $B1$ phase

Experimentally the most stable forms of the lithium and sodium fluorides and the magnesium and calcium oxides are the face-centered-cubic structures. Our results for these systems are given in Table II along with the CG results. Experimental values for the nearest-neighbor distances, R_e, and dissociation energies, D_e, are also provided. Where possible we have used data for 0 K in determining the experimental energies and report experimental values for R_e extrapolated to 0 K. In other cases we give experimental results for 298 K, since the temperature

TABLE II. Equilibrium geometries and dissociation energies for LiF, NaF, MgO, and CaO in the $B1$ phase.

Crystal		R_e(a.u.)[a]	$-W_B$(a.u.)[b]	D_e(a.u.)[c]	$\Phi_i(r_i)$[d]	$-N_i/r_0$[e]	r_0[f]
LiF $B1$	Two body, free ion[g]	4.03	0.3833	0.3833		0.0	∞
	Many body, free ion	4.071	0.3774	0.3774	0.430	0.0	∞
	Many body, SS ion, partly converged	3.884	0.4036	0.3969	0.450	0.435	2.30
	Many body, SS ion, self-consistent	3.854	0.4072	0.3979	0.454	0.465	2.15
	Experimental	3.806[h]		0.3933[i]			
NaF $B1$[j]	Two body, free ion[g]	4.61	0.3377	0.3377		0.0	∞
	Many body, free ion	4.638	0.3353	0.3353	0.372	0.0	∞
	Many body, SS ion, partly converged	4.504	0.3507	0.3475	0.388	0.378	2.65
	Many body, SS ion, self-consistent	4.490	0.3522	0.3482	0.389	0.392	2.55
	Experimental	4.378[h]		0.3472[i]			
MgO $B1$[j]	Two body, SS ion,[g] partly converged	4.33	1.388	1.119		0.376[k]	2.66
	Many body, SS ion, partly converged	4.338	1.3777	1.1087	0.813	0.376[k]	2.66
	Many body, SS ion, partly converged	4.120	1.4870	1.1484	0.850	0.833	2.40
	Many body, SS ion, self-consistent	4.101	1.4958	1.1510	0.853	0.851	2.35
	Experimental	3.955[l]		1.1571[m]			
CaO $B1$	Two body, SS ion,[g] partly converged	4.67	1.2988	1.0298		0.376[k]	2.66
	Many body, SS ion, partly converged	4.711	1.2907	1.0217	0.745	0.376[k]	2.66
	Many body, SS ion, self-consistent	4.568	1.3454	1.0302	0.765	0.756	2.646
	Experimental	4.545[n]		1.007[g]			

[a]Nearest-neighbor distance in atomic units.
[b]Difference between the total crystal energy per formula unit and the total self-energies of the cations and SS anions.
[c]Energy per formula unit necessary to separate the crystal into gas phase ions.
[d]Electrostatic potential at the nuclear position of the anion.
[e]Shell potential used in the SCF calculation.
[f]Shell radius in atomic units.
[g]Reference 7.
[h]Experimental value at 0 K, compiled by Tosi, Ref. 2.
[i]Kittel, Ref. 25, p. 121.
[j]Face-centered-cubic structure.
[k]Calculated from the wave function of Watson, Ref. 20, with $-N_i = 1.0$.
[l]Experimental value at 0 K, quoted by Cohen and Gordon, Ref. 7.
[m]Compiled from data in Ref. 26 at 0 K.
[n]Reference 11, at 298 K.

dependence of these quantities is small.

The precision of the numerical integrations is increased by basing the calculations on a primitive unit cell rather than the larger conventional cubic unit cell. For any face-centered-cubic lattice it is possible to perform the calculations using a rhombohedral unit cell[2] which occupies one-fourth the volume of the cubic cell. For the $B1$ phase calculations the angles between the lattice vectors were fixed at 60° and the length of the lattice vector $\vec{a}$ was varied in the energy minimization. In addition, the position of the anion in the unit cell was varied with the cation fixed at the origin. In all cases there was no significant deviation of the anion position from $(\frac{1}{2},\frac{1}{2},\frac{1}{2})$, which is in accord with the observed geometries.

In applying the correction factors of the MEG theory[6] to the many-body numerical integration of Sec. II, we have chosen to use the correction factors appropriate for the nearest-neighbor pair. Thus for NaF and MgO correction factors for a system of 20 electrons (16 valence) were used, while for LiF and CaO the correction factors for 12 and 28 electrons and 10 and 16 valence electrons, respectively, were used. For the first two systems the correction factors apply for the more distant neighbors as well. For LiF and CaO the chosen correction factors are intermediate between those appropriate for anion-anion and cation-cation second-nearest-neighbor interactions. For LiF results obtained with the correction factors for 20 electrons differed by less than 1% from the results reported in Table II for 12 electrons.

We may first examine the effects of the nonaddi-

tive many-body forces on the equilibrium geometry and energy in these crystals by comparing our results using gas phase F^- or Watson's[20] O^{2-} charge densities with the results of CG using the same densities. Generally, with these wave functions our model predicts a slightly smaller dissociation energy and a slightly larger nearest-neighbor distance at the minimum than the pairwise interaction model of CG. Except for the D_e value of CaO, this makes the agreement with the experimental geometries and dissociation energies worse than the CG results by a very small amount. The greatest change is in the results for LiF, where our D_e value is 1.5% smaller than the CG result.

There is a simple explanation for this effect. The many-body forces, in the electron-gas approximation, arise from the mutual overlap of three or more charge distributions. From the nonlinear form of the electron-gas energy functionals it is easily seen that this leads to the reduction in magnitude of each of the electron-gas interaction energies from the two-body results.[8] Near the equilibrium configuration of the crystal, the magnitude of the attractive exchange term is decreased the most. The net short-range potential is thus more repulsive, which increases the lattice parameter and reduces the dissociation energy.

We find that the electron-gas nonadditive many-body effects are small and lead to very little change in the results from two-body calculations. This may be a deficiency of the electron-gas model. In their study of He_3, Lloyd and Pugh[24] found that the electron-gas model seriously underestimated the magnitude of three-body interactions in this system. It should be noted, however, that the electron-gas theories generally give poorer results for systems with few electrons, such as helium, than for systems containing larger numbers of electrons. Conclusions based on the He_3 system cannot be assumed to apply to larger systems.

While the inclusion of many-body forces in the model leads to very small changes in the results, the use of the SS charge densities improves the agreement with experiment remarkably. In the case of LiF, the anion site potential of 0.430, obtained from the energy minimization with the gas phase F^- wave function, was used as a guide in selecting r_0 for the next SCF calculation. The new F^- density was more contracted than the gas phase density and when used in the next energy minimization gave significantly improved values of R_e and D_e. The smaller R_e value led to a higher anion site potential, and a final SCF calculation was performed with $r_0 = 2.15$. This new wave function was used in an additional energy minimization which gave convergence of R_e and D_e to less than a percent difference from their previous values. The anion site potential in the final minimization matched the shell potential to within 2.4%. While W_B continues to decrease as the degree of the shell stabilization is increased, this trend is opposed by the increase in the self-energy $(-W_B - D_e)$ of the F^- anion. The final (self-consistent) LiF result in Table II gives R_e and D_e differing by 1.3% and 1.2%, respectively, from the experimental values.[25,26] This is a considerable improvement over the CG results.

A similar procedure to that outlined above was followed for the remaining systems in Table II. The successive SCF calculations and energy minimizations were repeated until the potentials matched to within a few percent, there being little additional change in R_e and D_e after this. This criterion for self-consistency appears to be sufficiently stringent for our current purposes and requires only a few iterations before being met.

The pattern observed for NaF, MgO, and CaO is similar to that for LiF. The CG results for NaF gave an R_e value some 5.3% too large and D_e too small by -2.7%. The present model with $r_0 = 2.55$ reduces these errors to 2.6% and 0.3%, respectively. The results for MgO and CaO are similarly improved. For MgO the self-consistent result agrees with the experimental R_e by 3.7% and D_e by -0.5%, while for CaO the deviations for R_e and D_e in the self-consistent result are 0.5% and 2.3%, respectively. Overall for these systems the agreement with the experimental geometries and dissociation energies is as good as can be expected from a model that neglects long-range dispersion forces and lattice vibrations.

B. Properties of the $B2$ and $B3$ phases

A sensitive test of any solid-state theory is its ability to correctly predict the relative stabilities of different crystal structures. In this regard there are three highly symmetric cubic phases of interest. In the $B1$ phase, treated in the previous section, the ions are sixfold coordinated. Tetrahedral coordination is found in sphalerite or $B3$ structures, whereas in $B2$ or body-centered-cubic structures the ions are eightfold coordinated. The relative densities generally increase in the order $B3$-$B1$-$B2$ so that the $B2$ phase is most favored at high pressures.

A number of semiempirical theories[2,27] overestimate the stability of the $B1$ phase relative to the $B2$. Recently, it has been shown[27] that the same theories also predict that at zero pressure the $B3$ structure will be the most stable form of LiF and NaF rather than the $B1$ phase in which these compounds are actually found. To test our theory we have calculated the properties of the $B2$ and $B3$ phases of the systems treated in Sec. VI A. The results are given in Table III. The preferred structure at zero pressure is determined by the sign of ΔD_e, which is the difference between the calculated dissociation energy of the $B2$ or $B3$ phase and the $B1$ result. Differences were taken between results obtained from comparable

TABLE III. Calculated geometries and dissociation energies for the $B2$ and $B3$ phases of LiF, NaF, MgO, and CaO. Notation is the same as in Table II.

Crystal		R_e(a.u.)	D_e(a.u.)	$\Phi_i(r_i)$	$-N_i/r_0$	r_0	ΔD_e(kcal/mole)[a]
LiF $B2$[b]	Two body, free ion[c]	4.36	0.3568		0.0	∞	−16.6
	Many body, free ion	4.436	0.3505	0.399	0.0	∞	−16.9
	Many body, SS ion, self-consistent	4.240	0.3671	0.416	0.435	2.30	−19.3
LiF $B3$[d]	Many body, free ion	3.716	0.3836	0.440	0.0	∞	3.9
	Many body, SS ion, partially converged	3.564	0.4006	0.460	4.35	2.30	2.3
	Many body, SS ion, self-consistent	3.537	0.4014	0.463	4.60	2.15	2.2
NaF $B2$	Two body,[c] free ion	4.89	0.3237		0.0	∞	−8.8
	Many body, free ion	4.919	0.3206	0.359	0.0	∞	−9.2
	Many body, SS ion, self-consistent	4.745	0.3336	0.371	0.378	2.646	−9.2
NaF $B3$	Many body, free ion	4.340	0.3335	0.377	0.0	∞	−1.1
	Many body, self-consistent	4.252	0.3453	0.385	0.392	2.55	−1.8
MgO $B2$	Two body,[c] SS ion,[e] partially converged	4.59	1.0565		0.376	2.66	−39.2
	Many body, SS ion,[e] partially converged	4.598	1.0470	0.777	0.376	2.66	−38.7
	Many body, SS ion, self-consistent	4.379	1.0773	0.807	0.833	2.40	−46.2
MgO $B3$	Many body, SS ion,[e] partially converged	4.012	1.1161	0.824	0.376[e]	2.66	4.6
	Many body, SS ion, self-consistent	3.805	1.1490	0.861	0.851	2.35	−1.3
CaO $B2$	Two body,[c] SS ion,[e] partially converged	4.93	0.9801		0.376	2.66	−31.2
	Many body, SS ion,[e] partially converged	4.903	0.9773	0.725	0.376	2.66	−27.9
	Many body, SS ion, self-consistent	4.822	0.9776	0.732	0.756	2.646	−33.0
CaO $B3$	Many body, SS ion,[e] partially converged	4.355	1.0183	0.754	0.376	2.66	−2.1
	Many body, SS ion, self-consistent	4.261	1.0191	0.769	0.756	2.646	−7.0

[a]Difference in dissociation energy in kcal/mole between this result and the result for the $B1$ phase.
[b]Body-centered-cubic structure.
[c]Reference 7.
[d]Sphalerite structure.
[e]Calculated from the wave function of Watson, Ref. 20, with $-N_i = 1.0$.

wave functions, i.e., either the free ion F^- wave functions or Watson's O^{2-} wave function in both cases or SS wave functions that correspond to the self-consistent results in the respective structures.

With the exception of LiF, the present theory correctly predicts the $B1$ phase will be the most stable structure for these systems. Although we find that the $B2$ phase will be substantially less stable than the $B1$ phase in all cases, the $B3$ phase is seen to be surprisingly close in energy to the $B1$ structure, and in the case of LiF the $B3$ form is calculated to be the most stable structure. In contrast to most of the semiempirical theories considered by Narayan and Ramaseshan,[27] we get the correct result for NaF.

From the results for LiF and the rather small calculated energy differences between the $B3$ and $B1$ phases for the other systems, it appears likely that the present model, like the Born-Mayer models, overestimates the stability of the $B3$ phase. There are a number of physical effects neglected by or only partially accounted for in the theories that could explain this. We may examine these individually.

It has been suggested[13] that many-body forces are the determining factor in the relative stability of different crystal structures. In LiF, where the anions overlap considerably, this is likely to be more important than in the other systems we consider here. Comparing the present LiF results using a free F^- wave function with the CG results for the $B1$ and $B2$ phases, we see, however, that the nonadditive many-body effects in the MEG theory tend to destabilize the more dense $B2$ phase by 0.3 kcal/mole. For the relative stability of the $B3$ and $B1$ phases, the many-body forces probably favor the $B3$ phase rather than the $B1$ phase and are no doubt small.

The recent semiempirical theory[27] of Narayan and Ramaseshan (NR), in which the ions were treated as elastically compressible, but nonspherical, succeeds in

predicting the correct structures for all the alkali halides. The contraction of the anions, which we represent by the use of the SS charge densities, is a similar effect except that we constrain the ions to remain spherically symmetric. It is apparent from the results in Table III that the use of the SS charge densities does indeed stabilize the $B1$ phase relative to the $B3$. This can be viewed as a result of the effective increase in the cation-anion size ratio. In view of the NR results one might think that the nonspherical distortions would increase the stability of the $B1$ phase. This is doubtful, however, since nonspherical distortions are more probable in the more open $B3$ structure, and this effect would tend to stabilize the $B3$ relative to the $B1$.

Qualitative arguments based on cation-anion size ratios, suggest that a further contraction of the anion density would increase the stability of the $B1$ phase relative to the $B3$ and, perhaps, give the correct prediction for the most stable structure. In the present model, only the effect of the electrostatic portion of the crystalline environment is incorporated into the Hartree-Fock calculations. The valence electron density can overlap with the neighboring core densities in violation of the Pauli exclusion principle. The model could be further refined to estimate these overlap effects, by including an effective repulsive pseudopotential, representing the neighboring cores, in the Hartree-Fock calculations. This would lead to more contracted anion densities. However, the remarkably accurate results obtained from the present theory, suggest that anion contraction due to the overlap effects, has a relatively minor effect on the overall crystal energy and geometry.

The use of the GK correlation energy functional, Eq. (4c), to represent the dispersion or van der Waals's interactions is another possible source of error. The short-range pair potentials obtained by GK[5(a)] with this functional showed an exponential decay at large separations rather than the correct $-C_{ij}/R^6$ attraction. The theory presented here thus underestimates the attractive van der Waals's forces. Since these forces stabilize the more dense phases, this error could underestimate the stability of the $B1$ phase relative to the $B3$ phase.

Although accurate values for the C_{ij} coefficients for the ion-ion dispersion forces are not known, we can make reasonable estimates for the coefficients and the net dispersion energies in these crystals.

From a Drude model analysis[28] of the long-range dispersion forces in atoms the coefficient of the asymptotic potential for homonuclear pairs is found to be

$$C_{ii} = \tfrac{3}{4}\alpha_i^{3/2} N_i^{1/2} \ ,$$

where α_i is the electronic polarizability and N_i is the effective number of polarizable electrons. For the ionic systems considered here the crystal polarizabilities are known[29,30] and, following a suggestion in Ref. 28, we can take N_i to be the same as the value determined for the isoelectronic rare-gas pair. For the heteronuclear pairs the results in Ref. 28 also yield

$$C_{ij} = 2C_{ii}C_{jj}\alpha_i\alpha_j/(C_{ii}\alpha_j^2 + C_{jj}\alpha_i^2) \ .$$

Values for these coefficients are listed in Table IV. The result obtained for Li^+ in this way agrees well with the recent theoretical value[31] of $C_{ii} = 0.0783$ a.u. The remaining values are in fair agreement with earlier estimates.[2,11]

Once the coefficients are determined it is straightforward to determine the net van der Waals's energy

$$W_V = -C_{R_e}/R_e^6 \ ,$$

where R_e is the nearest-neighbor distance. For the cubic crystals under consideration here, C_{R_e} may be determined from values for the lattice sums given in

TABLE IV. van der Waals's coefficients. All quantities are given in a.u.

Ion pair	α_i	N_i[a]	C_{ij}
Li^+Li^+	0.1930[b]	1.433	0.076 12
Na^+Na^+	1.721[b]	3.940	3.3609
F^-F^-	5.122[b]	3.940	17.256
Li^+F^-			0.9838
Na^+F^-			7.3410
$Mg^{2+}Mg^{2+}$	0.6343[c]	3.940	0.7520
$Ca^{2+}Ca^{2+}$	7.8078[c]	5.506	38.940
$O^{2-}O^{2-}$	11.1820[c]	3.940	55.663
$Mg^{2+}O^{2-}$			5.100
$Ca^{2+}O^{2-}$			45.542

[a]Reference 28. [b]Reference 29. [c]Reference 30.

Ref. 2. The results of these calculations are listed in Table V. Since the dispersion forces are partially accounted for by the MEG correlation energy, a better estimate for the error in our results is W_V' in Table V, in which the contributions from the nearest neighbors have been subtracted from the total. The MEG correlation energy generally gives an adequate description of the van der Waals's effects from the nearest neighbors but underestimates the interactions with the next nearest neighbors. The errors in the dispersion energy in our results are seen from Table V to be less than 10 kcal/mole. If the effects of the next nearest neighbors are subtracted as well (W_V'' in Table V) the net result is small, which indicates that contributions beyond next nearest neighbors are minor.

The errors in the net dissociation energy that result from the MEG correlation energy are small, and at least for the lighter systems, will be largely canceled by the neglect of the zero-point energy in the calculations. For LiF and NaF in the $B1$ phase the total vibrational energy at 298 K is[2] 4.43 and 3.90 kcal/mole, respectively. Since this is well below the Debye temperature for these crystals, this should be a fair estimate of the zero-point energy. For MgO and CaO the zero-point energy has been calculated[32] to be 3.5 and 2.7 kcal/mole, respectively. Thus in the heavier systems the magnitude of the dispersion energy is considerably larger than the zero-point energy, and for these systems a better estimate of the dispersion energy may be necessary.

The errors in the present calculations from the sources discussed thus far lead to small errors in the dissociation energy. Their effect on the relative stability of the different phases may be more important since, as we have seen, the differences in energy between phases can be quite small. For the relative stability of the $B3$ and $B1$ phases the dispersion energy stabilizes the $B1$ phase by up to several kcal/mole. In the case of LiF, $\Delta W_V'$ in Table V is -1.236 kcal/mole and is not quite enough to give the correct order of stability of the two phases, with the dissociation energy of the $B1$ phase of LiF calculated to be a little less than 1 kcal/mole below that of the $B3$ phase. For the $B2$ and $B1$ structures a more accurate description of the dispersion energies reduces the relative stability of the $B1$ phase by several kcal/mole. Although this does not change the order of stability at zero pressure, it may have an important effect on the high-pressure behavior.

The relative stability of the different phases will also be affected by differences between the zero-point energies in the different structures. This is difficult to estimate quantitatively. The zero-point energy is probably lower in the structures of lower density. When the zero-point energy is large, as in LiF, this would favor the $B3$ phase over the $B1$, canceling effects due to dispersion forces. In the heavier systems the zero-point-energy differences will be smaller and of less consequence.

TABLE V. van der Waals's energies in different phases. All energies are in kcal/mole.

Crystal	r_0[a]	R_e[b]	$-W_V$[c]	$-W_V'$[d]	$-W_V''$[e]	ΔW_V[f]	$\Delta W_V'$[f]	$\Delta W_V''$[f]
LiF $B1$	2.15	3.854	4.241	3.109	0.611			
$B2$	2.30	4.240	4.242	3.425	1.007	0.002	0.316	0.395
$B3$	2.15	3.537	3.490	2.228	0.484	−0.751	−1.236	−0.127
NaF $B1$	2.55	4.490	5.134	1.761	0.441			
$B2$	2.646	4.745	5.523	2.274	0.911	0.389	0.513	0.470
$B3$	2.55	4.252	4.228	1.111	0.418	−0.906	−0.650	−0.023
MgO $B1$	2.35	4.101	11.160	7.123	1.541			
$B2$	2.40	4.379	12.851	9.220	2.866	1.690	2.097	1.325
$B3$	2.35	3.805	9.036	4.819	1.128	−2.124	−2.304	−0.413
CaO $B1$	2.646	4.568	26.613	7.740	2.868			
$B2$	2.646	4.822	28.119	9.932	3.990	1.506	2.192	1.122
$B3$	2.646	4.261	24.548	5.451	2.330	−2.065	−2.290	−0.538

[a]Shell radius.
[b]Nearest-neighbor distance.
[c]Total van der Waals's energy.
[d]van der Waals's energy minus nearest-neighbor contributions.
[e]van der Waals's energy minus first- and second-nearest-neighbor contributions.
[f]Difference between van der Waals's energy in $B1$ phase and $B2$ or $B3$ phase.

VII. RESULTS FOR BeF_2, MgF_2, CaF_2, AND Na_2O

In this section we consider results for three of the alkaline earth fluorides and sodium oxide. These systems are well suited for the application of the present theory since they are highly ionic and are found in structures of relatively high symmetry. First, we examine the calculated results for the geometries and dissociation energies for these systems in their experimentally determined structures. The many-body results are compared to two-body calculations obtained by a generalization of the methods of Ref. 7 to more complex crystal structures. The experimental structures again provide examples of four-, six-, and eightfold coordination of the cations. Next, as a further test of the theory, we consider the relative stabilities of alternative crystal structures for these systems.

A. Results for BeF_2

BeF_2 has a high-temperature modification with the high cristobalite structure.[33] As a first approximation this crystal type is based on a fcc lattice with the ions in sites of high symmetry. Since this is a high-temperature phase, it is likely that the reported atomic positions represent an average over sites of lower symmetry about which the ions vibrate.

A primitive rhombohedral unit cell was again used in the calculations for this system. Cations were placed in the positions (0,0,0) and $(\frac{1}{4},\frac{1}{4},\frac{1}{4})$, while anions in the basis were placed at $(\frac{1}{8},\frac{1}{8},\frac{1}{8})$, $(\frac{5}{8},\frac{1}{8},\frac{1}{8})$, $(\frac{1}{8},\frac{5}{8},\frac{1}{8})$, and $(\frac{1}{8},\frac{1}{8},\frac{5}{8})$ with respect to the primitive unit-cell axes. In order to reduce the computation time in the calculations, the atomic positions were not varied in the minimization; the only variable parameter was the length of the unit-cell axis.

The free ion results for BeF_2, in Table VI, show that the nonlinear many-body effects in this system act to increase the dissociation energy and reduce the length of the lattice axis. Thus at the small interatomic distances encountered in this system the dominant nonlinear many-body effect is the reduction of the kinetic interaction energy. Both free ion results give rather poor agreement with the experimental[26,33] values of these quantities. On the other hand, the self-consistent results obtained with the SS ions are in extremely close agreement with the experimental results, which is surprising considering the high electronegativity of beryllium compared to the metals considered previously.

B. Results for MgF_2

Crystalline MgF_2 is found to have the same structure as rutile.[33] This is a structure with a somewhat lower symmetry than the cubic structures considered thus far, but since the polarizability of the F^- anion is small, polarization effects in this crystal should be of minor importance. The unit cell is tetragonal and contains two formula units. The Mg^{2+} ions are located at (0,0,0) and $(\frac{1}{2},\frac{1}{2},\frac{1}{2})$, while the anion positions are given by $(\pm u, \pm u, 0)$ and $(\frac{1}{2}\pm u, \frac{1}{2}\mp u, \frac{1}{2})$. The parameter u determines the equilibrium anion position within an isosceles triangle formed by the cations. In the calculations reported in Table VI the lengths of the $\vec{a}$ and $\vec{c}$ axes were varied along with the parameter u.

The results for MgF_2 again demonstrate the significant improvement obtained from the use of the SS densities instead of free ion densities. Both the two-body and many-body free ion results for the lengths of the lattice axes show rather large positive deviations from the experimental results and the calculated dissociation energies in these cases are too small. The many-body results give a slightly larger unit cell volume and smaller dissociation energy than the two-body results, which is the effect found in the previous section. Since the site potentials in MgF_2 (and BeF_2) are significantly larger than the site potentials typical of the alkali fluorides, the F^- ions in MgF_2 and BeF_2 are considerably more contracted than in NaF and LiF. As a result the unit cell volume of MgF_2 calculated from gas phase wave functions by the many-body method is 21.7% larger than the experimental value. The self-consistent result obtained with an SS density gives a unit-cell volume that is only 2.9% larger than the experimental value and the calculated dissociation energy is only 0.15% smaller than the experimental value. This difference can hardly be regarded as significant.

C. Results for CaF_2 and Na_2O

The fluorite structures of CaF_2 and Na_2O are well known,[2,25] and it is again possible to base the calculations on a primitive rhombohedral unit cell. In these calculations the length of the unit-cell axis was varied in the minimization. In addition, for CaF_2 the cation position was fixed at the origin and the coordinates of both the F^- anions were varied in the search for the minimum energy. For Na_2O the same procedure was followed with the cation and anion positions reversed. Again no significant deviations from the experimentally determined positions of $(\frac{1}{4},\frac{1}{4},\frac{1}{4})$ and $(\frac{3}{4},\frac{3}{4},\frac{3}{4})$ were found. The results of these calculations are included in Table VI.

The results for these systems are similar to those observed previously. For both systems, the nonlinear many-body effect is primarily a reduction of the exchange energy. The self-consistent result for CaF_2 gives a dissociation energy slightly greater than the experimental value at 298 K. The greater calcu-

TABLE VI. Equilibrium geometries and dissociation energies for BeF_2, MgF_2, CaF_2, and Na_2O in four-, six-, and eightfold-coordinate structures. Notation is the same as in Table II.

System	Structure		$\|\vec{a}\|$[a] (a.u.)	$\|\vec{c}\|$[a] (a.u.)	u	$-W_B$ (a.u.)	D_e (a.u.)	$\Phi_i(\vec{r}_i)$	$-N_i/r_0$	r_0	ΔD_e[b] (kcal/mole)
BeF_2	High cristobalite	Two body, free ion	10.098	···	···	1.2256	1.2256	0.567	0.0	∞	
	High cristobalite	Many body, free ion	9.960	···	···	1.2362	1.2362	0.575	0.0	∞	
	High cristobalite	Many body, SS ion, self-consistent	9.175	···	···	1.3803	1.3161	0.622	0.625	1.6	
	High cristobalite	Experimental	9.060[c]	···	···		1.3238[d]				
BeF_2	Rutile	Many body, SS ion, self-consistent	7.921	4.992	0.310	1.2663	1.2343	0.530	0.526	1.9	−51.3
	CdI_2	Many body, SS ion, self-consistent	5.231	8.362	0.180	1.2280	1.1959	0.554	0.526	1.9	−75.4
	Fluorite	Many body, SS ion, self-consistent	6.259	···	···	1.1656	1.1471	0.461	0.465	2.15	−106.0
MgF_2	Rutile	Two body, free ion	9.163	6.213	0.304	1.0600	1.0600	0.441	0.0	∞	
	Rutile	Many body, free ion	9.271	6.231	0.304	1.0507	1.0507	0.437	0.0	∞	
	Rutile	Many body, SS ion, self-consistent	8.797	5.852	0.305	1.1265	1.1079	0.463	0.465	2.15	
	Rutile	Experimental	8.736[c]	5.767	0.303		1.1095[e]				
	High cristobalite	Many body, SS ion, self-consistent	11.383	···	···	1.1293	1.1035	0.501	0.500	2.0	−2.8
	CdI_2	Many body, SS ion, self-consistent	6.076	8.787	0.180	1.0954	1.0766	0.472	0.465	2.15	−19.6
	Fluorite	Many body, SS ion, self-consistent	6.763	···	···	1.0907	1.0773	0.426	0.435	2.30	−19.2
CaF_2	Fluorite	Two body, free ion	7.560	···	···	0.9731	0.9731	0.382	0.0	∞	···
	Fluorite	Many body, free ion	7.544	···	···	0.9707	0.9707	0.383	0.0	∞	···
	Fluorite	Many body, SS ion, self-consistent	7.412	···	···	1.0029	0.9949	0.389	0.392	2.55	···
	Fluorite	Experimental	7.300[c]	···	···	···	0.9918[d]	···	···	···	···
CaF_2	High cristobalite	Many body, SS ion, self-consistent	12.916	···	···	0.9963	0.9828	0.442	0.435	2.30	−7.6
	Rutile	Many body, SS ion, self-consistent	9.792	6.548	0.310	1.0174	1.0065	0.415	0.417	2.40	7.3
	CdI_2	Many body, SS ion, self-consistent	6.961	8.939	0.185	0.9782	0.9673	0.406	0.417	2.40	−15.4
Na_2O	Antifluorite	Two body, SS ion, partially converged	7.7198			0.9215	0.6525	0.693	0.375[f]	2.66[f]	
	Antifluorite	Many body, SS ion, partially converged	7.784	···	···	0.9166	0.6476	0.688	0.375[f]	2.66[f]	
	Antifluorite	Many body, SS ion, self-consistent	7.606	···	···	0.9503	0.6470	0.703	0.714	2.8	
	Antifluorite	Experimental	7.42[c]				0.6602[g]				
	High cristobalite	Many body, SS ion, self-consistent	13.644	···	···	0.9175	0.6143	0.648	0.714	2.8	−20.5
	Rutile	Many body, SS ion, self-consistent	10.045	7.085	0.311	0.9420	0.6387	0.692	0.714	2.8	−5.2
	CdI_2	Many body, SS ion, self-consistent	7.364	10.142	0.153	0.9279	0.6247	0.658	0.714		−14.0

[a]Length of primitive unit-cell axis.
[b]Difference between calculated dissociation energies of this phase and the phase found experimentally at zero pressure.
[c]Reference 33.
[d]Calculated from data in Ref. 26 for 298 K.
[e]Calculated from data in Ref. 26 for 0 K.
[f]Calculated from wave function of Watson (Ref. 20) with $-N_i = 1.0$.
[g]Calculated from the data in Ref. 34 for 298 K.

lated value is in part due to the neglect of vibrational energy in the model and is similar to what was observed for CaO.

For Na_2O, many-body calculations using Watson's[20] O^{2-} wave function gave a lattice constant 4.9% too large and a dissociation energy that was too small by 1.9%. The use of an SS density led to a significant improvement in $|\vec{a}|$ and a very slight decrease in D_e.

D. Alternative structures for BeF_2, MgF_2, CaF_2, and Na_2O

The relative stability of possible alternative structures for the alkaline earth fluorides and Na_2O can be determined in a manner similar to that of Sec. VI. In the sequence BeF_2, MgF_2, and CaF_2, in the experimentally determined structures, the cation coordination number passes from four to six to eight. Thus, a useful test for the theory is to consider each of these compounds and Na_2O in the high cristobalite, rutile, and fluorite structures. An additional structure of interest here is the CdI_2-type hexagonal lattice in which the cations are also sixfold coordinated. Here the unit cell contains a cation at the origin with anions at $(\pm\frac{1}{3}, \pm\frac{2}{3}, \pm u)$. The parameter u, along with the lengths of the two lattice axes $\vec{a}$ and $\vec{c}$, was varied in the energy minimization.

For BeF_2, the results in Table VI indicate that the four-coordinate cristobalite structure is correctly found to be much more stable than any of the structures exhibiting a higher coordination number. For MgF_2, the rutile structure is correctly predicted to be the most stable, but the dissociation energy for the high cristobalite structure is very close to rutile result. The CdI_2 and fluorite structures are substantially less stable than either of these. The model incorrectly predicts that a rutile-type structure for CaF_2 will be 7.3 kcal/mole more stable than the observed fluorite structure. A more exact treatment of the dispersion energies would lower this difference, but in view of the results in Sec. VI, it is unlikely that it could reverse the order of stability. The antifluorite structure is correctly predicted to be most stable in Na_2O, but a sixfold coordination of the oxide anions is seen to be rather close in energy to the eightfold structure. In no case is the CdI_2-type structure competitive with the rutile-type structures for these ionic compounds. Once again, in the case of MgF_2 and CaF_2, the model seems to predict excessive stability for the structures of lower coordination number.

E. Pressure induced phase transitions in MgF_2

The prediction[7(b)] of a phase transition in CaO,[35] has proven to be an important application of the electron-gas theory. In a recent experiment,[36] it has been shown that at high pressure rutile MgF_2 undergoes a structural transformation to a denser, distorted fluorite-type structure. In this section, as an additional test of the present theory, we compare calculated results on MgF_2 at high pressure with these experimental results.

Since the observed high-pressure phase in MgF_2 appears to be only a small distortion from a true fluorite structure,[36] the pressure dependence of the free-energy difference between the rutile and undistorted fluorite structures was calculated. Energy differences between the distorted and undistorted fluorite forms should be small. In the static lattice approximation, the free energy, G, and equilibrium geometry of a given phase at pressure P is obtained by minimizing

$$G = -D_e + PV \ ,$$

where V is the volume per formula unit, with respect to the structural parameters. Calculations using both the many-body and two-body models were performed at a series of pressures up to 700 kbar. Since the anion site potential increases as the lattice is compressed, more highly stabilized wave functions, consistent with the higher site potentials, were used at the higher pressures. The calculated compression curves for both phases appear in Fig. 2, along with the experimental results.[36]

The overall agreement between the theoretical and experimental pressure-volume curves is good, although the calculated unit-cell volumes are generally too large. Nonlinear many-body effects are different in the two structures. For the rutile form the many-body results give a more contracted lattice than the two-body results. The opposite effect occurs in the fluorite phase where the two-body model leads to

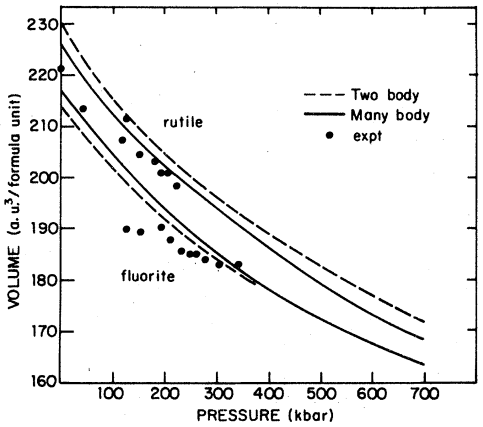

FIG. 2. Pressure-volume curves for MgF_2 in the rutile and fluorite structures. Experimental points are from Ref. 36.

a denser crystal. The calculated percent volume change at the experimental transition pressure is 5.5% and 5.0% in the two- and many-body calculations, respectively, and agrees well with the experimental value of 5%.

The transition pressure is found from the point at which the free energies of the two phases are the same. At 296 K the experimental transition pressure is found to be ~ 300 kbar,[36] and, from the temperature dependence of the transition pressure, at 0 K a transition should be observed at ~ 325 kbar. The calculated transition pressures were found to vary widely with small changes in the model. A two-body calculation with $r_0 = 2.15$ for both phases gives a transition pressure of ~ 430 kbar. Since the site potential in the rutile form is higher than in the fluorite, another, more refined, calculation was performed with $r_0 = 2.0$ for the rutile structure and $r_0 = 2.15$ for the fluorite. This gives better agreement with the site potentials at higher pressures and a slight stabilization of the rutile phase occurs. This causes a large change in the transition pressure, however, increasing it to ~ 650 kbar. Larger errors occur when the many-body model is applied to these structures. No transition is found in the regime of 0 to 700 kbar. Extrapolation of the calculated free energy curves gives a transition pressure of about 1500 kbar for the many-body calculation.

The different nonlinear many-body effects in the two phases arise from the variation of the many-body forces with distance and differences in the nearest-neighbor distances in the two structures. At very short separations the dominant many-body interaction is a reduction of the repulsive kinetic energy term, while at longer distances the reduction of the attractive exchange interaction is most significant. In the rutile form of MgF_2 nearest-neighbor distances are shorter than in the fluorite structure. This leads to a higher site potential in rutile MgF_2. In addition, this means that as the lattice is compressed, the primary many-body effect is the reduction of the net kinetic energy and greater stabilization of the lattice. In fluorite MgF_2, however, the nearest-neighbor distance is longer than in the rutile structure and there are a greater number of more distance neighbors. This causes a net reduction of the exchange energy and an increased repulsion in the many-body calculations. A net destabilization of the fluorite phase relative to the rutile results.

This overall behavior may be incorrect because of the neglect of long-range dispersion forces in both the two-body and many-body calculations. These interactions lead to a smaller lattice and an increased relative stability of the more dense phase and so would tend to cancel the many-body effects. Thus a more accurate calculation of the phase relationships should include both dispersion and many-body effects, although in view of the results of Sec. V, it is unlikely that this would greatly alter the results. On the other hand, it can be argued that the simpler two-body model, neglecting both dispersion and many-body forces, is more appropriate for the calculation of phase relationships than the use of many-body forces, including dispersion.

Although the two-body model gives better agreement with the experimental transition pressures than the many-body model, it still underestimates the stability of the fluorite phase. Since the density of the two phases is also too small, it may be that an additional stabilization, and consequent shrinkage, of the anion density is required. In addition to improving the agreement with experimental densities, this should increase the stability of the fluorite phase by increasing the effective cation to anion size ratio.

Although further refinements of the theory are required before transition pressures can be calculated accurately, the present methods can give reasonable predictions of the likelihood of transitions between two phases. The pressure-volume curves and the volume change at transition can be predicted with acceptable accuracy.

VIII. SUMMARY AND CONCLUSIONS

The modified electron-gas theory, incorporating several many-body effects, presented here gives excellent results for the geometry and dissociation energy of highly symmetric ionic crystals. Stabilization of the anion wave functions by a simple electrostatic model leads to significant improvements in the calculated results over previous methods. The nonlinear many-body effects included in the theory are smaller and of less importance. The model is sometimes deficient in its ability to predict the relative stability of various crystal structures and seems to favor structures of lower coordination number in a number of cases. Errors of this type appear to be due to factors other than simple dispersion forces; it may be necessary to include the effect of Pauli type, nearest-neighbor repulsions in the determination of the anion wave function.

When applied to the prediction of pressure-induced phase transitions, the model appears to again underestimate the stability of the higher density modification, which leads to overestimation of the transition pressure. Volume changes on transition and calculated compressibility curves agree reasonably well with experiment.

ACKNOWLEDGMENTS

One of us (C.W.M.) would like to thank Dr. Alan Cohen and Dr. Marvin Waldman for many useful and illuminating discussions and Dr. Richard Stevens

for a great deal of programming assistance. We are grateful to Professor William Lipscomb, Dr. Edward Laws, and the programmers of Walpole State Prison for the use of their atomic SCF program. This work was supported in part by the National Science Foundation, Grants No. CHE-7708324 and No. PCM 77-11398, and the Materials Research Laboratory at Harvard University.

APPENDIX: POINT COULOMB POTENTIALS AND INTERACTION ENERGIES IN IONIC CRYSTALS

The Ewald double sum formula[15] is a very efficient method for the evaluation of point Coulomb site potentials and Madelung energies in ionic crystals. In this section we generalize the method to the case where the lattice of Gaussian functions introduced by Ewald is replaced by a lattice of arbitrary functions with density given by Eq. (19). In the Ewald method all the Gaussians are assumed to have the same halfwidths; here we allow the functions $\sigma_j(\vec{y})$ to vary at different sites in the unit cell. This results in some small modifications to the formulas given by Ewald.

First let us derive a rapidly convergent expression for the point Coulomb or Madelung potential

$$\Phi_M(\vec{x}) = \sum_j \sum_{\vec{l}} \frac{N_j}{|\vec{x} - \vec{r}_{jl}|} \quad . \tag{A1}$$

The notation is the same as in Sec. II. Consider a lattice of spherically symmetric charge distributions for which the net charge density is

$$\rho'_M(\vec{y}) = \sum_j \sum_{\vec{l}} N_j \sigma_j(\vec{y} - \vec{r}_{jl}) \quad . \tag{A2}$$

This is similar to Eq. (19) with the Q_j replaced by the ionic charges N_j. The electrostatic potential in this lattice is

$$\Phi'_M(\vec{x}) = \sum_j \sum_{\vec{l}} N_j \int d\vec{y}\, \frac{\sigma_j(\vec{y} - \vec{r}_{jl})}{|\vec{x} - \vec{y}|}$$

$$= \sum_j \sum_{\vec{l}} N_j H_j(\vec{x} - \vec{r}_{jl}) \quad , \tag{A3}$$

where $H_j(\vec{x})$ is defined by Eq. (25).

An expansion for $\Phi'_M(\vec{x})$ in the reciprocal lattice can also be found. Since $\rho'_M(\vec{x})$ is periodic, it has the Fourier series representation

$$\rho'_M(\vec{y}) = V^{-1} \sum_{\vec{k}} B(\vec{k}) e^{-i\vec{k}\cdot\vec{y}} \quad , \tag{A4}$$

where $\vec{k}$ is a reciprocal-lattice vector. The expansion coefficients are given by

$$B(\vec{k}) = \sum_j N_j \sum_{\vec{l}} \int_V d\vec{y}\, e^{i\vec{k}\cdot\vec{y}} \sigma_j(\vec{y} - \vec{r}_{jl})$$

$$= \sum_j N_j e^{i\vec{k}\cdot\vec{r}_j} \int d\vec{y}\,' e^{i\vec{k}\cdot\vec{y}'} \sigma_j(\vec{y}') \quad ,$$

where, as in Sec. II, the lattice sum and integration over a single unit cell has been converted into an integration over all space. We have also made use of the relation $e^{i\vec{k}\cdot\vec{r}_l} = 1$ which defines the reciprocal lattice. Since the $\sigma_j(\vec{y})$ are normalized and the unit cell is neutral $B(0) = 0$.

The lattice potential is found by solving Poisson's equation

$$\nabla^2 \Phi'_M(\vec{x}) = -4\pi \rho'_M(\vec{x})$$

with Eq. (A4) for $\rho'_M(\vec{x})$ to obtain

$$\Phi'_M(\vec{x}) = C + 4\pi V^{-1} \sum_{\vec{k}}{}' B(\vec{k}) \frac{e^{-i\vec{k}\cdot\vec{x}}}{k^2} \quad , \tag{A5}$$

where C is a constant and we exclude the $\vec{k} = 0$ vector from the sum. If we require the average potential in a unit cell, calculated from Eq. (A5), to be the same as the average potential calculated by integrating Eq. (A3) over a unit cell we find that

$$C = V^{-1} \sum_j N_j \sum_{\vec{l}} \int_V d\vec{x}\,' H_j(\vec{x}\,' - \vec{r}_{jl})$$

$$= V^{-1} \sum_j N_j \int d\vec{x} H_j(\vec{x}) \quad . \tag{A6}$$

Note that if all the $\sigma_j(\vec{y})$ are identical as in the original Ewald method this term vanishes. It is convenient to define

$$G_j(\vec{x}) = H_j(\vec{x}) - \frac{1}{x} \tag{A7}$$

as the nonpoint Coulomb part of $H_j(\vec{x})$. This then gives for the point Coulomb potential, Eq. (A1),

$$\Phi_M(\vec{x}) = \Phi'_M(\vec{x}) - \sum_j \sum_{\vec{l}} N_j G_j(\vec{x} - \vec{r}_{jl}) \quad .$$

The substitution of Eq. (A5) into this expression then yields

$$\Phi_M(\vec{x}) = C + 4\pi V^{-1} \sum_{\vec{k}}{}' B(\vec{k}) \frac{e^{-i\vec{k}\cdot\vec{x}}}{k^2}$$

$$- \sum_j \sum_{\vec{l}} N_j G_j(\vec{x} - \vec{r}_{jl}) \quad . \tag{A8}$$

For reasonable choices of the $\sigma_j(\vec{y})$ each of the summations will be rapidly convergent.

If we consider a lattice with a defect at $\vec{x} = \vec{r}_i$, the electrostatic potential is

$$\Phi'_i(\vec{x}) = \Phi_M(\vec{x}) - N_i/|\vec{x} - \vec{r}_i| = C + 4\pi V^{-1} \sum_{\vec{k}} B(\vec{k}) \frac{e^{-i\vec{k}\cdot\vec{x}}}{k^2} - \sum_j \sum_{\vec{l}}{}' N_j G_j(\vec{x} - \vec{r}_{jl}) - N_i H_i(\vec{x} - \vec{r}_i) \quad , \tag{A9}$$

where the term $\vec{r}_l = 0$ is excluded from the direct lattice sum if $i = j$. The Madelung energy, Eq. (11), may be found from Eq. (A9) since

$$W_M = \tfrac{1}{2} \sum_i \int d\vec{x} N_i \delta(\vec{x} - \vec{r}_i) \Phi_i'(\vec{x}) \ .$$

When Eq. (A9) is substituted into this expression and the integration is performed, the result is Eq. (39). The constant term in the potential adds nothing to the interaction energy because of the neutrality of the lattice. For completeness we give the explicit results when the $\sigma_j(y)$ are chosen to be Gaussians as in Eq. (38). The electrostatic potential is then given by

$$H_j(x) = (2/\sqrt{\pi}) \int_0^{\alpha_j x} dy\, e^{-y^2}/x = \frac{\mathrm{erf}(\alpha_j x)}{x}$$

and the Fourier expansion coefficient is

$$B(\vec{k}) = \sum_j N_j e^{i\vec{k}\cdot\vec{r}_j} e^{-k^2/4\alpha_j^2} \ .$$

Both of these functions will fall off rapidly with distance for a wide range of values. Finally, we note that in this case

$$H_i(0) = 2\alpha_j/\sqrt{\pi}$$

and

$$C = -\pi \sum_j N_j / V \alpha_j^2 \ .$$

[1] M. Born and K. Huang, *Dynamic Theory of Crystal Lattice* (Oxford University Press, London, 1954).
[2] M. P. Tosi, Solid State Phys. 16, 1 (1964).
[3] P. O. Löwdin, Ph.D. thesis (Uppsala, 1948) (unpublished).
[4] J. L. Calais, Int. J. Quantum Chem. Symp. 9, 497 (1975).
[5] (a) R. G. Gordon and Y. S. Kim, J. Chem. Phys. 56, 3122 (1972). (b) Y. S. Kim and R. G. Gordon, Phys. Rev. B 9, 3548 (1974).
[6] M. Waldman and R. G. Gordon, J. Chem. Phys. 71, 1325 (1979).
[7] (a) A. J. Cohen and R. G. Gordon, Phys. Rev. B 12, 3228 (1975). (b) A. J. Cohen and R. G. Gordon, Phys. Rev. B 14, 4593 (1976).
[8] Y. S. Kim, Phys. Rev. A 11, 796 (1975).
[9] W. C. Mackrodt and R. F. Stewart, J. Phys. C 12, 431 (1979).
[10] B. G. Dick and A. W. Overhauser, Phys. Rev. 112, 90 (1958).
[11] S. Cantor, J. Chem. Phys. 59, 5189 (1973).
[12] E. S. Gaffney and T. J. Ahrens, J. Chem. Phys. 51, 1088 (1969).
[13] L. Jansen and E. Lombardi, Discuss. Faraday Soc. 40, 78 (1965).
[14] R. A. LeSar and R. G. Gordon (unpublished results).
[15] P. P. Ewald, Ann. Phys. (Leipzig) 64, 253 (1921).
[16] F. Bertaut, J. Phys. Radium 13, 499 (1952).
[17] C. B. Haselgrove, Math. Computation 15, 323 (1961).
[18] H. Conroy, J. Chem. Phys. 47, 5307 (1967).
[19] E. Pachalis and A. Weiss, Theor. Chim. Acta 13, 381 (1969).
[20] R. E. Watson, Phys. Rev. 111, 1108 (1958).
[21] E. Laws and the Walpole Computer Programmers, Atomic SCF Program, 1971.
[22] E. Clementi and C. Roetti, At. Data. Nucl. Data Tables 14, 177 (1974).
[23] E. Clementi, J. Chem. Phys. 38, 2248 (1963).
[24] J. Lloyd and D. Pugh, Chem. Phys. Lett. 54, 65 (1978).
[25] C. Kittel, *Introduction to Solid State Physics,* 4th ed. (Wiley, New York, 1971).
[26] (a) D. D. Wagman, W. H. Evans, V. B. Parker, I. Halow, S. M. Bailey, and R. H. Schumm, Tech. Note U.S. Natl. Bur. Stand. 170-3 (1968) (unpublished). (b) V. B. Parker, D. D. Wagman, and W. H. Evans, Tech. Note U.S. Natl. Bur. Stand. 270-6 (1971) (unpublished).
[27] R. Narayan and S. Ramaseshan, Phys. Rev. Lett. 42, 992 (1979).
[28] Y. S. Kim and R. G. Gordon, J. Chem. Phys. 61, 1 (1974).
[29] J. R. Tessman, A. H. Kahn, and W. Shockley, Phys. Rev. 92, 890 (1953).
[30] I. M. Boswarva, Phys. Rev. B 1, 1698 (1970).
[31] R. M. Glover and F. Weinhold, J. Chem. Phys. 66, 191 (1977).
[32] E. Gmelin and S. Viera, Z. Naturforsch. A 27, 605 (1972).
[33] R. W. G. Wyckoff, *Crystal Structures,* 2nd ed. (Wiley, New York, 1963), Vol. 1.
[34] *Handbook of Chemistry and Physics,* 60th ed., edited by R. C. Weast (CRC, Boca Raton, 1979).
[35] R. Jeanloz, T. J. Ahrens, H. K. Mao, and P. M. Bell, Science 206, 829 (1979).
[36] L. C. Ming and M. H. Manghani, Geophys. Res. Lett. 6, 13 (1979).